

Conformational transitions of heteropolymers in dilute solutions

E.G. Timoshenko*, Yu.A. Kuznetsov, K.A. Dawson

*Theory and Computation Group, Irish Centre for Colloid Science and Biomaterials[†],
Department of Chemistry, University College Dublin, Belfield, Dublin 4, Ireland
(February 1, 2008)*

In this paper we extend the Gaussian self-consistent method to permit study of the equilibrium and kinetics of conformational transitions for heteropolymers with any given primary sequence. The kinetic equations earlier derived by us are transformed to a form containing only the mean squared distances between pairs of monomers. These equations are further expressed in terms of instantaneous gradients of the variational free energy. The method allowed us to study exhaustively the stability and conformational structure of some periodic and random aperiodic sequences. A typical phase diagram of a fairly long amphiphilic heteropolymer chain is found to contain phases of the extended coil, the homogeneous globule, the micro-phase separated globule, and a large number of frustrated states, which result in conformational phases of the random coil and the frozen globule. We have also found that for a certain class of sequences the frustrated phases are suppressed. The kinetics of folding from the extended coil to the globule proceeds through non-equilibrium states possessing locally compacted, but partially misfolded and frustrated, structure. This results in a rather complicated multistep kinetic process typical of glassy systems.

PACS numbers: 36.20.-r, 87.15.-v

I. INTRODUCTION

Study of the conformational transitions of heteropolymers in dilute solutions is important for many applications from the chemical industry to biotechnology. Directed more towards the former, there has been a significant amount of theoretical work carried out on concentrated copolymer solutions, mixtures and blends [1–9] using various types of the density formalism. However, these approaches are not valid at infinitely low dilution where the fundamental interactions of the individual macromolecule determine its conformational state. This situation is more relevant for biochemistry. The problem is even harder to address at non-equilibrium conditions typical for biopolymers *in vivo* [10].

For these reasons we have been working for some time on developing an adequate statistical mechanical technique for studying the equilibrium structure and kinetics across phase transitions in heteropolymers [11–13]. The main idea was to extend the Gaussian self-consistent (GSC) method, originally proposed for the homopolymer (see e.g. [14] and references therein), to the case of inhomogeneous monomer interactions. This has been achieved in Ref. [11] where we have derived the complete set of non-linear kinetic equations for complex valued equal-time correlation functions of the Fourier transforms of the monomer coordinates. There we have analysed in some detail the simplest periodic (ab) copolymer, but study of more complicated sequences remained out of our practical computational reach. The relation of the kinetic equations to the equilibrium free energy, as well as the expression for the entropy, were also unknown to us at that stage. Thus, the phase diagram have not been elucidated and certain other important issues have not been addressed in that work.

In the following two works [12,13] we have achieved further progress and resolved most of these questions, though at the cost of losing detailed information about individual sequences. Namely, we have performed averaging of the GSC equations over the quenched disorder in the monomer amphiphilic strength. This yielded a closed set of kinetic equations for description of random copolymers with a Gaussian distribution of the disorder. Such an idealised system is very interesting in itself, particularly since there is a hope that its study could shed light on some features of the extremely complex problem of protein folding [10].

To render the quenched disorder problem more tractable certain perturbative approximation was necessary [12]. It became clear in Ref. [13] that this causes some deficiencies in the equilibrium limit of the formalism, and we have alluded as to how these could be alleviated in higher orders of the expansion.

*Corresponding author. Internet: <http://fiachra.ucd.ie/~timosh>

[†]Established at the University College Dublin and Queen's University of Belfast

Therefore, it seems important to revisit the general formalism of Ref. [11] in order to resolve remaining difficulties, maintaining the rich information about particular sequences and avoiding any further approximations. Furthermore, there exists, till now, no simple theoretical procedure capable of giving the equilibrium conformational states of a heteropolymer with arbitrary sequence, that can in a consistent manner also give the full kinetic pathway between these states. The work presented here achieves this. To demonstrate the strength of the extended GSC method we consider a number of interesting examples of heteropolymer sequences. Different kinds of interactions, such the hydrodynamic interaction, may be straightforwardly incorporated into the scheme. A rich and nontrivial physical picture emerges as a result of this theoretical progress.

II. THE BEAD-AND-SPRING MODEL

Traditionally, we proceed from the coarse-grained description of the polymer chain [2–4] with the spatial coordinates \mathbf{X}_n ascribed to the n -th monomer. It is assumed that the long timescale evolution of conformational changes is well represented by the phenomenological Langevin equation, which upon neglecting the backflow effect of the solvent may be written as,

$$\zeta_b \frac{d}{dt} \mathbf{X}_n = - \frac{\partial H}{\partial \mathbf{X}_n} + \boldsymbol{\eta}_n(t), \quad (1)$$

where ζ_b is the “bare” friction constant per monomer. For the discussion of the hydrodynamic interaction we refer the reader to Appendix A. The thermal fluctuations are incorporated via the Gaussian noise which, according to the Einstein law, is characterised by the second momentum,

$$\langle \eta_n^\alpha(t) \eta_{n'}^{\alpha'}(t') \rangle = 2k_B T \zeta_b \delta^{\alpha, \alpha'} \delta_{n, n'} \delta(t - t'), \quad (2)$$

where the Greek indices denote the spatial components of 3-d vectors.

In the current treatment the solvent is effectively excluded from the consideration [15] and the resulting monomer interactions are described by the effective free energy functional,

$$H = \frac{k}{2} \sum_n (\mathbf{X}_n - \mathbf{X}_{n-1})^2 + \frac{\varkappa}{2} \sum_n (\mathbf{X}_{n+1} + \mathbf{X}_{n-1} - 2\mathbf{X}_n)^2 + \sum_{J=2}^{\infty} \sum_{\{n\}} u_{\{n\}}^{(J)} \prod_{i=1}^{J-1} \delta(\mathbf{X}_{n_{i+1}} - \mathbf{X}_{n_1}), \quad (3)$$

where in principle $u_{\{n\}}^{(J)}$ are allowed to have any dependence on the site indices $\{n\} \equiv \{n_1, \dots, n_J\}$.

The first two terms in Eq. (3) describe the connectivity and the stiffness of the chain. Their coefficients have the following simple meaning: $k = k_B T / l^2$ and $\varkappa = k_B T \lambda / l^3$ with l and λ called the statistical segment length and the persistent length [4,16] respectively. Apart from these interactions, local along the chain, there are also long-range volume interactions represented by the virial-type expansion [2,3] in Eq. (3). The latter reflects the hard core repulsion and weak attraction between monomers, but also the effective interaction mediated by the solvent–monomer couplings I_n .

The coefficients in this expansion may be calculated as functions of the temperature and the parameters of molecular interaction. However, for our purposes we do not need to know their explicit form here as we shall keep only a few first terms. Appropriate coefficients then may be viewed as independent phenomenological parameters which could be directly related to experimentally measurable quantities.

In Refs. [11,13] we have discussed that the case of amphiphilic heteropolymers, for which monomers differ only in the monomer–solvent coupling constants, corresponds to the following choice of site-dependent second virial coefficients in Eq. (3),

$$u_{nn'}^{(2)} = \bar{u}^{(2)} + \frac{1}{2}(I_n + I_{n'}), \quad \sum_n I_n = 0. \quad (4)$$

The mean second virial coefficient $\bar{u}^{(2)}$ is associated with the quality of the solvent: positive values correspond to the good solvent (where effective two-body repulsion of monomers results in the extended coil conformation), and the negative values correspond to the bad solvent condition (where the effective two-body attraction tends to compact the chain).

The set of couplings $\{I_n\}$ expresses the chemical composition, or using the biological terminology, the primary sequence of a heteropolymer. For simplicity, in the consequent sections we shall consider examples for which these

constants can be parametrised in a simple way: $I_n = \Delta \sigma_n$, where variables σ_n can only take three values: $-1, 1$ or 0 corresponding to (a) hydrophobic, (b) hydrophilic and (c) “neutral” monomers respectively. The parameter Δ is called the degree of amphiphilicity of the chain. Note that for more complicated than binary sequences there is another relevant dispersion, $(\Delta_\sigma)^2 = \frac{1}{N} \sum_m \sigma_m^2$, and the combination $\Delta \Delta_\sigma$ is a more appropriate variable.

III. THE GSC KINETIC EQUATIONS

In work [11] we have derived a set (18) of the GSC kinetic equations for the equal-time correlation functions of the Fourier transforms of monomer coordinates $\mathcal{F}_q^{AA'}(t)$. There, at the end of Sec. II, we have mentioned that a polymer with no periodic structure may be described by choosing the number of blocks $M = 1$. The equations for the correlation functions,

$$\mathcal{F}_{mm'}(t) \equiv \frac{1}{3} \left\langle \mathbf{X}_m(t) \mathbf{X}_{m'}(t) \right\rangle, \quad (5)$$

contain some redundancies and also are intermixed with the diffusive degree of freedom describing the motion of the centre-of-mass. Obviously, for a single chain the latter can be easily decoupled from the intra-molecular degrees of freedom by introducing the mean squared distances between pairs of monomers,

$$D_{mm'}(t) \equiv \frac{1}{3} \left\langle (\mathbf{X}_m(t) - \mathbf{X}_{m'}(t))^2 \right\rangle = \mathcal{F}_{mm} + \mathcal{F}_{m'm'} - 2\mathcal{F}_{mm'}. \quad (6)$$

It turns out that from Eq. (18) in Ref. [11] after certain algebraic manipulations one can obtain a closed set of equations for the quantities $D_{mm'}(t)$.

Taking into account the additional bending energy contribution in Eq. (3), the GSC equations may be written down in the most general form as follows,

$$\begin{aligned} \frac{\zeta_b}{2} \frac{d}{dt} D_{mm'} &= 2k_B T (1 - \delta_{mm'}) + k(D_{mm',m+1m} + D_{mm',m-1m} + (m \leftrightarrow m')) \\ &\quad - \mathfrak{a}(D_{mm',m+2m+1} + D_{mm',m-2m-1} - 3D_{mm',m-1m} - 3D_{mm',m+1m} + (m \leftrightarrow m')) \\ &\quad + \sum_{J=2}^{\infty} \sum_{\{n\}} \frac{\hat{u}_{\{n\}}^{(J)}}{(\det \Delta^{(J-1)})^{5/2}} \sum_{i,j=1}^{J-1} \bar{\Delta}_{ij}^{(J-1)} (\delta_{n_1}^m + \delta_{n_{i+1}}^{m'} - \delta_{n_{i+1}}^m - \delta_{n_1}^{m'}) D_{mm',n_1 n_{j+1}}, \end{aligned} \quad (7)$$

where we have introduced the four-point correlation functions, $D_{mm',nn'}$, and the matrix $\Delta_{ij}^{(J-1)}$ of size $(J-1)$ with the cofactor $\bar{\Delta}_{ij}^{(J-1)}$,

$$D_{mm',nn'} \equiv -\frac{1}{2} (D_{mn} + D_{m'n'} - D_{mn'} - D_{m'n}), \quad (8)$$

$$\Delta_{ij}^{(J-1)} \equiv D_{n_1 n_{i+1}, n_1 n_{j+1}}. \quad (9)$$

Similarly to Eq. (31) in Ref. [11] for the mean energy $\mathcal{E} = \langle H \rangle$ we have,

$$\begin{aligned} \mathcal{E} &= \frac{3k}{2} \sum_n D_{nn-1, n n-1} + \frac{3\mathfrak{a}}{2} \sum_n (2D_{n+1 n, n+1 n} + 2D_{n-1 n, n-1 n} - D_{n-1 n+1, n-1 n+1}) \\ &\quad + \sum_{J=2}^{\infty} \sum_{\{n\}} \hat{u}_{\{n\}}^{(J)} (\det \Delta^{(J-1)})^{-3/2}. \end{aligned} \quad (10)$$

It is interesting to note that in the case of the homopolymer the right-hand side of the kinetic equations (7) may be rewritten via the instantaneous gradients of the variational free energy by introducing the normal modes (see Eq. (5) in Ref. [17]). This establishes connection of the stationary limit of our kinetic approach with the equilibrium theory, in which we recover the Gibbs–Bogoliubov variational principle. We also note that if first order phase transitions are involved, one has to possess the expression for the free energy in order to determine the phase boundaries by finding the global free energy minimum.

The variational free energy, \mathcal{A} , based on the Gaussian *Ansatz* for equal-time pair correlation functions, contains two terms, $\mathcal{A} = \mathcal{E} - T\mathcal{S}$. Naturally, the mean energy term is given by Eq. (10). The second, entropic contribution, is

calculated in Appendix B. Let us summarise the result of that calculation here. One representation for the entropy that is suitable for numerical analysis is,

$$\mathcal{S} = \frac{3}{2} k_B \log \det R^{(N-1)}, \quad (11)$$

where we have used the determinant of the $(N-1)$ -dimensional major submatrix of the matrix,

$$R_{nn'} = \frac{1}{N^2} \sum_{mm'} D_{nm,n'm'} = -\frac{1}{2} \Lambda^0 \bullet D \bullet \Lambda^0, \quad (12)$$

and the matrix D obviously has the elements equal to $D_{nn'}$. The reason for appearance of the truncated matrix is that we have excluded the zero eigenvalue of R related to the translational invariance. Here we have also introduced the $(N-1)$ -dimensional orthogonal projector Λ^0 such that,

$$(\Lambda^0)^2 = \Lambda^0, \quad (\Lambda^0)^T = \Lambda_0, \quad \sum_n (\Lambda^0)_{nk} = 0, \quad (13)$$

with the matrix elements $(\Lambda^0)_{nk} = \delta_{n,k} - 1/N$. This matrix has obviously one zero eigenvalue and $N-1$ degenerate eigenvalues equal to 1.

However, for analytical treatment it is more convenient to obtain a slightly different expression by regularising the zero eigenvalue (i.e. by imposing the constraint $\sum_n \mathbf{X}_n = 0$ as a “soft” condition in Eq. (B1)),

$$\mathcal{S} = \frac{3}{2} k_B \lim_{\epsilon \rightarrow 0} \log \frac{\det(R + \epsilon \mathbf{1})}{\epsilon}. \quad (14)$$

Since the matrix $(R + \epsilon \mathbf{1})$ is nondegenerate we can easily differentiate Eq. (14) so that,

$$Q_{ik} \equiv \lim_{\epsilon \rightarrow 0} \sum_j D_{ij} \frac{\partial}{\partial D_{kj}} \text{Tr} \log(R + \epsilon \mathbf{1}) = \sum_j D_{ij} \text{Tr}_0 \left(\frac{\partial R}{\partial D_{kj}} \bullet R_0^{-1} \right) = (\Lambda^0)_{ik}, \quad (15)$$

where inside the trace Tr_0 over the $(N-1)$ -dimensional subspace projected out by Λ^0 the matrix R becomes invertible with the inverse denoted as R_0^{-1} . This allows us to obtain the combination which appears in the kinetic equations,

$$Q_{ii} + Q_{kk} - Q_{ik} - Q_{ki} = 2(1 - \delta_{i,k}). \quad (16)$$

These preliminaries are sufficient to prove the desired relation. Indeed, using Eq. (16) by direct and tedious differentiation of Eq. (10) one can show that the kinetic equations (7) may be expressed through the instantaneous gradients [18] of the variational free energy as,

$$\zeta_b \frac{d}{dt} D_{mm'}(t) = -\frac{2}{3} \sum_{m''} (D_{mm''}(t) - D_{m'm''}(t)) \left(\frac{\partial \mathcal{A}[D(t)]}{\partial D_{mm''}(t)} - \frac{\partial \mathcal{A}[D(t)]}{\partial D_{m'm''}(t)} \right). \quad (17)$$

This formula, together with Eqs. (10,14), is the key formal result of the current work. The structure of Eq. (17) is sufficiently nontrivial to be guessed from phenomenological arguments and has been derived in a systematic manner proceeding from Eq. (7).

We would like to comment here that although, for simplicity, we have presented the explicit formulae above for a ring polymer, our current formalism is general and covariant. In fact, the kinetic equations (17) are valid for any topology of the chain. Thus, it is straightforward to consider more complicated topologies such as a star, brush, network, branched chain and so on. For that it is sufficient to modify only the spring and stiffness terms in Eq. (3), and respectively in Eq. (10). For example, to describe an open chain one has simply to suppress the term with $n = 0$ in the connectivity contribution, and the terms with $n = 0, N-1$ in the stiffness contribution to the energy. We undertake a detailed comparison of ring versus open homopolymers in kinetics at the collapse transition of the homopolymer in a separate work [19]. Another interesting possibility is that the general equation (17) is also valid for models with different ways of representing the connectivity and stiffness. For example, the freely rotating model [4] can be obtained by suppressing the first two terms in Eq. (10) and instead keeping fixed the following mean squared distances: $D_{m,m+1} = b_0^2$ and $D_{m,m+2} = 4b_0^2 \sin^2 \theta / 2$, where b_0 and θ are the bond length and angle. This is easy to prove by adding appropriate “soft” constraints to the free energy functional and taking the consequent limit in Eq. (17), so that they become delta-functions in the partition function.

Finally, let us introduce two main observables: the mean squared radius of gyration and the degree of micro-phase separation [12],

$$R_g^2 = \frac{1}{2N^2} \sum_{mm'} D_{mm'}, \quad \Psi = \frac{1}{N^2 R_g^2 \Delta \Delta_\sigma} \sum_{mm'} (u_{mm'}^{(2)} - \bar{u}^{(2)}) D_{mm'}. \quad (18)$$

The second parameter has a meaning of the dimensionless correlation of the matrices of the relative two-body interaction and the mean squared distances. For heteropolymers with two types of monomers it characterises the difference between the mean squared radii of gyration of hydrophilic and hydrophobic species, and for the symmetric composition with their numbers equal we have a simple relation: $\Psi = (R_g^2(b) - R_g^2(a))/(2R_g^2)$.

IV. NUMERICAL RESULTS

The self-consistent kinetic equations (17) have been studied numerically using the explicit formulae (C1,C2,C4) for the effective potentials (see Appendix C), and the expression given by the first term in the right-hand side of Eq. (7) for the entropic contribution. We used the fifth order adaptive step Runge-Kutta method [20] to improve stability of the solution which, for large amphiphilicity parameter, Δ , is characterised by a rather rugged free energy landscape. We note that such kinetic method for finding the equilibrium distributions is more reliable and efficient than the standard methods of free energy minimisation if there are lots of mountains and valleys on its surface. We also refrain from study of the influence of the hydrodynamics in this paper for the analysis and results are complicated enough already. Besides, the hydrodynamics in the preaveraged approximation does not affect the equilibrium state, which is recovered by taking the stationary limit in the kinetic equations.

We include the volume interactions up to the three-body terms only, i.e. $u_{\{n\}}^{(J)} = 0$ for $J > 3$. As can be seen from Eqs. (17,C2) the computational time per time step scales with the chain length as $t_c \sim N^3$ here. This performance is intermediate between that of the homopolymer $t_c \sim N^2$ [14,17] and that of the random copolymer $t_c \sim N^4$ [12,13]. The performance of the formalism in Ref. [11] was $t_c \sim K^4 M^2$, where K and M are the block length and number of blocks respectively. Besides, that formalism relied on the use of complex variables, and the unitary transformation to the real basis was not an easily automatised task for complicated sequences. Moreover, the treatment of the diffusive mode was nontrivial and sequence dependent. Thus, in every respect, the current scheme is most attractive for study of heteropolymer sequences from the computational point of view.

It is natural to work here with combinations $\mathcal{L} = (k_B T/k)^{1/2}$ and $\mathcal{T} = \zeta_b/k$ as the units of size and time. We choose $k = 1$, $k_B T = 1$ and $\zeta_b = 1$ to fix \mathcal{L} and \mathcal{T} equal to unity. In addition, we fix the following interaction parameters: the third virial coefficients $u_{mm'm''}^{(3)} = 10 k_B T \mathcal{L}^6$ and the stiffness $\kappa = 0$ as we did in Ref. [11].

Now, we turn to discussion of concrete results. We have studied ring chains of the lengths $N = 30, 60, 90$. We shall present here the most complete results for $N = 60$ and discuss the N dependence only briefly. We have examined many different sequences. However, we present our data in this paper only for three particular choices which we found most typical and illustrative of the heteropolymer behaviour. These are chains of: 30 (ab) blocks, 10 (aaabbb) blocks and 2 (abacbbcabccbaaacbccbbaacbcc) blocks, which we call the “short” blocks, “long” blocks and “random” sequences respectively (see the end of Section II for the monomer notations).

A. Equilibrium phase diagrams

The phase diagrams in terms of the mean second virial coefficient \bar{u}_2 and the amphiphilicity Δ for the above mentioned three sequences are presented in Figs. 1-3. For positive values of $\bar{u}_2^{(2)}$ and comparatively small values of Δ the conformational state of the chain is akin to a homopolymer extended coil (see Fig. 4a). By decreasing $\bar{u}_2^{(2)}$ to the negative region the chain is caused to undergo a continuous (second-order-like) collapse transition (curve (C)), that is characterised by a rapid fall of the radius of gyration [21] (see Fig. 1 of Ref. [14]) and the change of the fractal dimension. Proceeding from the collapsed globule at a fixed negative $\bar{u}_2^{(2)}$ the increase of the amphiphilicity Δ also causes a continuous transition (curve (S)) to the micro-phase separated (MPS) globule [22]. During this transition the system size, R_g , monotonically increases (see Fig. 5) and the mean energy \mathcal{E} decreases in agreement with our earlier results in Refs. [23,11]. The former change is more pronounced for the “long” blocks compared to other sequences, for which the connectivity constraints impede formation of structures with a hydrophilic shell and hydrophobic core. The MPS order parameter Ψ (see Fig. 6) increases almost linearly for small Δ , then after the transition asymptotically saturates.

The transition from the coil at large values of Δ to the MPS globule turns out to be more complicated, and essentially dependent on the sequence. In case of the “long” blocks (Fig. 2) the collapse transition to the MPS globule becomes discontinuous (first-order-like). Thus, inside the boundaries of metastability, designated by spinodals I' and I'', there are two competing minima of the free energy: the coil and the MPS globule. The former minimum is characterised by a large size, R_g , (on the right of Fig. 7) and a small MPS order parameter Ψ (Fig. 8), while for the latter minimum the situation is reversed (see the left hand side of Figs. 7,8). The depths of the free energy minima become exactly equal on the transition curve I in Fig. 2.

For the “short” blocks (Fig. 1), as well as for many random sequences (such as in Fig. 3), the phase diagram is much more complicated. Starting from some value of Δ and for intermediate values of $\bar{u}^{(2)}$ there appear additional solutions corresponding to local minima of the free energy. The broad region where this could take place is bounded by the curves I' and II'' in Figs. 1,3. With increasing Δ the number of such solutions grows quickly. Significantly, in a region of the phase diagram some of these become the main free energy minimum. As the number of such solutions grows roughly exponentially with the chain length, we do not attempt to draw all their boundaries of (meta)stability. Instead, we shall designate them collectively as *frustrated* phases, explaining this terminology below.

An important point here is that, as our analysis shows, these solutions become dominant in a narrow region of the phase diagram due to a subtle competition between the mean energy and the entropy. The MPS globule is entropically unfavourable there because the overall shrinking force is insufficiently strong. The values of R_g^2 and Ψ are intermediate for these solutions and lie between those of the coil and MPS globule (see Figs. 9,10). In this sense, we can call them nonfully compacted and misfolded states. In comparison, the MPS globule (see Fig. 4d) has a more compact size and better optimised volume interactions, what is manifested in a higher value of Ψ .

Most interesting is the local structure of these additional phases. Let us discuss the particular example of the 30(ab) sequence. The formalism of Ref. [11] has used heavily the assumption of certain symmetries for the mean squared distances $D_{mm'}$ due to which these variables can take only $3M$ independent values, where M is the number of blocks. These symmetries are: the block translation invariance,

$$D_{m+Ki, m'+Ki} = D_{m, m'}, \quad \text{for any } m, m' \text{ and } i, \quad (19)$$

where K is the block length, and the more complicated inversion symmetry discussed in detail in Ref. [11]. These symmetries have a simple meaning — a renumbering of monomers does change the average properties over the statistical ensemble — the interactions of a ring chain remain the same. However, the maximal possible number of dynamical variables in the GSC method is much larger and equals to $N(N-1)/2$. Surprisingly, it turns out that the frustrated phases are characterised by spontaneous breaking of these symmetries, and therefore only the current version of the method that takes into account all degrees of freedom can describe them. Thus, the property (19) is no longer valid. This phenomenon describes formation of local frustrated heterogeneities (see Figs. 4b,c) in which pieces of the chain form MPS clusters [23] that are prevented from further coalescing by their hydrophilic shells and high entropic barriers.

The role of spontaneous symmetry breaking is well recognised in equilibrium statistical mechanics. What is striking here is that the number of distinct spontaneously broken states becomes huge for large system sizes. This diversity and a special foliating structure of various branches leads in the thermodynamic limit to what is known as a spin glass like frozen phase [24] of random copolymers (see e.g. Refs. [12,13] and numerous references therein). We shall return to the issue of spontaneous symmetry breaking in kinetics in subsection IV B.

Even though the kinematic symmetries are not present from the outset for arbitrary, or random, sequences, the structure of the phase diagram (Fig. 3) and behaviour of main observables (Figs. 9,10) remain very similar. It is the particular structure, number and the shape of boundaries of frustrated phases that are very sensitive to the sequence. The symmetry that may be broken in this case has a subtler, dynamic, meaning and may be expressed in terms of the replica formalism [24]. In a sense, for a very long periodic chain, blocks may be viewed as identical copies of a smaller block-length chain. Thus, it is by no means surprising that the replica symmetry breaking in our case for periodic systems takes such an explicit manifestation in the breaking of the block translational symmetry. This important point was completely missed, nor could it be discovered, in our considerations of Ref. [11]. Therefore we have achieved here a new significant insight into the problem by a simple extension of the GSC method.

An interesting feature of our phase diagrams is that the region between spinodals I' and II'', designating where the frustrated phases can exist, expands dramatically with increasing chain length. For example, at $\Delta = 25$, for the 15(ab) sequence it lies approximately between $-19 < \bar{u}^{(2)} < 10$, while for the 30(ab) — between $-39 < \bar{u}^{(2)} < 11$, and the curve II'' goes nearly vertically downwards for larger N . According to the above interpretation, for infinitely long chain somewhere in this broad region and close to its boundaries there are the actual glass transition curves, which should be determined using proper glass order parameters. Thus, for short chains the curves I' and II'' may be viewed as approximate indicators of the freezing transitions. The former distinguishes between the homopolymer-like and the random coil, while the latter — between the homopolymer-like (liquid) and the frozen globules. As for the region

of stable MPS globule, it gets relatively smaller for larger systems. That is not surprising — the frustrated phases expand and the phase separation involving larger spatial scales requires stronger interactions. Having understood the identifications for the spinodals, we now can recognise in Figs. 1,3 the main features of the phase diagram, though rather distorted, of random copolymer model presented in Ref. [13].

Finally, let us comment on the phase diagram of the “long” blocks (Fig. 2). The micro-phase separation is obviously easier in this case and it dominates for large values of Δ , so that the frustrated phases are suppressed. We found that, qualitatively, in order to form a frustrated phase, in a finite range of Δ values, the number of (not necessarily identical) pieces of the chain with competing interactions should be larger than some critical number, in principle, weakly dependent on N . Here are a few examples conforming to this qualitative criterion: the phase diagram of 10(ab) behaves roughly as for 10(aaabbb), but for 15(ab) it behaves similarly to 30(ab); while for 15(aabb) the phase diagram looks like for 15(aaabbb) at small and moderate values of Δ , it becomes as for 30(ab) for much larger values of the amphiphilicity. It is reasonable to conjecture therefore that for a large number of (aaabbb) blocks, as well as for extremely high values of Δ and just 10 blocks, the frustrated phases may be found again.

B. Folding kinetics

Here we shall consider the time evolution of the conformational state of the system away from its initial equilibrium after it has been subjected to an instantaneous temperature jump that causes the two-body interaction parameters $\bar{u}^{(2)}$ and Δ to change. We are interested in quenches from the homopolymer coil, where all monomers are equally hydrophilic ($\bar{u}^{(2)} > 0$ and $\Delta = 0$), to the region of parameters corresponding to the MPS globular state, so that the ‘a’ species became strongly hydrophobic and the ‘b’ species remained weakly hydrophilic ($\bar{u}^{(2)} \ll 0$ and $\Delta \gtrsim |\bar{u}^{(2)}|$).

The temporal behaviour of the mean squared radius of gyration, $R_g^2(t)$, the MPS parameter, $\Psi(t)$, and the instantaneous free energy, $\mathcal{A}(t)$, in kinetics of folding for different sequences is presented in Figs. 11-13. For the homopolymer (curves (A)) R_g^2 and \mathcal{A} decrease monotonically to their final equilibrium values, while the MPS parameter, Ψ , remains identically zero for there is no distinction between different monomer species. These curves agree with the earlier results of Ref. [14] and serve for reference purpose here.

Now let us discuss the curves (B) corresponding to the periodic (ab) sequence. In the previous subsection we have mentioned that the current formalism yields results consistent with those of Ref. [11] only beyond the parameter region of the frustrated phases, which are characterised by spontaneous breaking of the block symmetry. In kinetics the situation is somewhat similar, but the consistence with the previous simplified formalism is even more limited. Really, the mean squared radius of gyration remains close to that of the “effective” homopolymer (curve (A)) during the first kinetic stage (see Eq. (74) in Ref. [11]). Interestingly, this is not quite so for more complicated sequences. The MPS parameter, $\Psi(t)$, for the (ab) copolymer grows slowly in a way similar to the splitting of the Fourier modes $\mathcal{F}_q^{11}(t) - \mathcal{F}_q^{00}(t)$ for large indices q (see Fig. 4 in Ref. [11]). However, contrary to the strange conclusion in Ref. [11] that the kinetics of the (ab) copolymer proceeds faster than for the homopolymer, we now have a, natural from the point of view of Monte Carlo simulations [23], slowing down of copolymer kinetics. Analysis of $D_{mm'}(t)$ shows that this effect is entirely due to the spontaneous breaking of the block symmetry in kinetics, something that has not been accounted for in Ref. [11]. Indeed, in Fig. 14 we exhibit the time dependence of the mean squared distances between two nearest hydrophobic monomers $D_{2k,2k+2}(t)$ for the (ab) copolymer in kinetics after a quench to the MPS globule region. For early, as well as for late, times these functions for different k are exactly equal to each other. However, there is well defined intermediate period in time where the block symmetry is spectacularly broken (see Fig. 15). We remark that the symmetry breaks and restores in a step-like manner (e.g. $D_{0,2}$ and $D_{4,6}$ join together at $t \simeq 10$, earlier than with other functions) and also that this effect is relatively strong.

We would like to make a general comment here on the nature of spontaneous symmetry breaking in kinetics. Thus, normally in such situations at equilibrium there exist a thermodynamically unstable symmetric free energy minimum and a disjoint set of symmetry broken minima, which may be transformed to each other by the residual subgroup of symmetry transformations. These states may also be obtained kinetically as infinite time limits of the time evolution starting from any, for example, the symmetric initial state, which happens to be the main free energy minimum before the quench.

However, the formal structure of the GSC kinetic equations (17) is such that they yield a symmetric solution at any moment in time provided one proceeds from the symmetric initial condition. A question arises then — how can one obtain the kinetics that could lead eventually to the multitude of final states with broken symmetry? The answer is clear in the exact theory — there are fluctuations that can transform between different spontaneously broken states in kinetics.

The GSC method presents, though an optimised and improved, but still a mean field type theory, where such fluctuations are not properly included. Manifestation of the kinetic spontaneous symmetry breaking takes a different

form there. Namely, at some moment in time the symmetric solution of the kinetic equations becomes unstable with respect to perturbations (whether of the initial condition, or of the interaction matrix, $u_{nn'}^{(2)}$). Thus, for example, one can add an infinitesimal symmetry breaking term $\varepsilon_{nn'}$ to the two-body interaction matrix and consider the limit of vanishing perturbation in the solution. Different choices of the form of $\varepsilon_{nn'}$ in the unperturbed limit would yield all possible types of spontaneously broken kinetic evolution, which are, of course, equivalent to each other. Numerically, such a regularisation procedure is not even necessary. There is always an intrinsic perturbation due to computer round off and numerical integration errors. Thus, if the symmetry is favourable to be kinetically broken somewhere, numerically one obtains one of the spontaneously broken solutions there, rather than the unstable symmetric solution, unless the symmetry conditions have been imposed by hand. In this situation improvement of the numerical precision would have no profound effect — the kinetic process either does not change, or can change only up to an experimentally unobservable residual symmetry transformation.

We note also that such a procedure of perturbing the interaction matrix here is analogous to introducing an external magnetic field in the Ising model. The spontaneous magnetisation of a macroscopic sample of ferromagnet may be achieved by gradually switching off the external magnetic field. In the absence of the field there would remain domains with long-range order, but varying directions of the spontaneous magnetisation canceling each other. Unfortunately, in our case it is not evident how to experimentally implement an analogous gradual switching off of $\varepsilon_{nn'}$.

Now returning to our results, in Fig. 11 one can see that the folding kinetics for the (ab) copolymer is about 3 times slower than for the homopolymer of the same length, the effect being even stronger for other sequences we have considered. From Fig. 12 and the phase diagrams in Figs. 1-3 it is evident that the considered quench results in the final state of the MPS globule for the “long” blocks (curve (C)), whereas in the frustrated phases for two other sequences (curves (B) and (D)). For the latter phases the MPS parameter is smaller and the radius is larger than for the MPS globule, as we already know from the equilibrium considerations. It is interesting to note that the final relaxation to the frustrated phases may be rather unusual. For example, in Figs. 11,12 for the “random” sequence $R_g^2(t)$ increases and $\Psi(t)$ decreases during the last kinetic stage, what is the converse to the behaviour at final relaxations in other cases. Another unusual observation is that for some sequences the parameter Ψ may even become negative during some time in kinetics, something we never observed at equilibrium. This shows that the structure of non-equilibrium conformations can be very complicated.

The instantaneous free energy $\mathcal{A}(t)$ depicted in Fig. 13 turns out to be the quantity most sensitive to the conformational structure of the non-equilibrium state. From that figure it strikes that, while the homopolymer folding is a single smooth relaxational process, the folding of heteropolymers proceeds through a multistep acceleration-deceleration process. The flat regions of a staircase-like function correspond to temporary kinetic arrest of the system in transient non-equilibrium (mostly symmetry broken) conformations. Generally speaking, in the GSC method we deal with the time evolution of a statistical ensemble of various initial conformations. The flat regions appear due to transient trappings of various members of the ensemble in their local shallow energy minima. Since such minima are encountered at different moments in time for different members of the ensemble, their influence on the overall time evolution of averaged observables is manifested in a smooth characteristic slowing down.

Qualitatively then, summarising the data for various sequences, most of which we have suppressed here, we can say that the number of local minima affects the number of stair steps, whereas the depth of minima determines the lengths of the steps. This interpretation is highly supported by the strong dependence of the stair case structure on the chain length, the sequence and the interaction parameters, for it is known how the frequency and depths of local potential energy minima depend on these factors. On the one hand, it is known that for a long heteropolymer chain the number of local minima grows exponentially with the chain length N , and indeed we see that the number of steps in $\mathcal{A}(t)$ grows just as quickly. On the other hand, increasing of the amphiphilicity, Δ , leads to higher depths of local minima as well as an increase in their number, and really the steps in $\mathcal{A}(t)$ become longer and more numerous. Let us give another example of such connection. For the “long” blocks the interactions are less frustrated than, say, for the (ab) blocks, thus there are much fewer of local energy minima, but the barrier between the coil and MPS globule is a higher. As a result, the kinetic process (curve (C) in Fig. 13) proceeds through only one rather long kinetically arrested step.

It is worthwhile to make a comment here on the notion of kinetic stages introduced in earlier works [25,14,23]. Those we associated with typical structures of the conformation and accompanying kinetic laws. We distinguished at least the following kinetic stages at the collapse of the homopolymer: early time necklace formation, middle time coarsening and a number of final relaxational processes. The multistep character of folding observed in this work affects the middle kinetic stage, resulting in its considerable complication and splitting into multiple substages with respective complex kinetic laws that are determined by the sequence. Universality of such kinetic laws is doubtful, but probably it can be recovered by averaging over certain classes of sequences with similar folding properties.

Apparently, in the GSC method the kinetics is a motion in the space of $N(N-1)/2$ averaged dynamic variables, $D_{nn'}(t)$, and it is determined by the profile of the free energy. It may be instructive, using Figs. 11 and 13, to present

the kinetics via a parametric plot of \mathcal{A} vs R_g , the latter being the main, though not the only, relevant “coordinate” of the system. That would produce a kind of “bottleneck” picture that was much discussed by P. Wolynes and others [26] in relation to the protein folding problem. This indicates that our method produces behaviour that permits interpretation in terms of phenomenological energy landscape models.

Finally, let us utilise once again the connection between the kinetic evolution of the free energy and the ruggedness of the potential energy landscape. This would allow us to shed some light on the general structure of the energy landscape for complex heteropolymers. Thus, a typical example of the “random” sequence kinetics (curve (D) in Fig. 13) shows first a fast drop, then appearance of short steps that are growing longer with time, until the last step becomes infinite. This translates to the following equivalent energy landscape versus some collective coordinate: first there is a rapid drop away from the unstable coil state, then the surface flattens and small wrinkles appear on it, they are growing larger in the amplitude gradually becoming high mountains and deep valleys, until there is eventually a very deep ravine corresponding to the “ground” state of the system separated by a very high barrier from other minima. In our view, the latter picture bears a remarkable resemblance to a typical mean field energy landscape in spin glass systems [24] recently discussed by G. Parisi [27]. This observation seems encouraging to us and indicates that the GSC method is capable of describing very complex systems, though it is too detailed and expensive in the complete form for description on a macroscopic scale. Nevertheless, by taking the quenched disorder averaging (similarly to Ref. [12]) it is possible to achieve an adequate description for heteropolymers that is alternative to the replica formalism. We believe that the underlying connection between both types of approaches has been clarified to some extent by the current work.

V. CONCLUSION

In the present work we have extended the Gaussian self-consistent method to permit study of heteropolymers with complicated primary sequences. This has been achieved by transforming the kinetic GSC equations, earlier derived for the Fourier modes, to the form containing only the mean squared distances between pairs of monomers and relating these equations to the instantaneous gradients of the variational free energy calculated based on the Gibbs–Bogoliubov principle. The revised GSC formalism possesses important computational advantages, but also it is fundamentally superior to its predecessor in that it can describe phenomena of spontaneous symmetry breaking and formation of structural heterogeneities.

We then have applied the extended GSC method to some particular amphiphilic heteropolymers. The equilibrium phase diagrams for these have been obtained in a systematic manner. Apart from the coil and two globular states we have discovered that in a wide intermediate region of the phase diagram there may be a large number of frustrated partially misfolded states. Despite the fact that such states, the number of which grows exponentially with the chain length, are mostly metastable, some of them become the dominant state in their rather narrow domains. The corresponding potential energy profile of the system has strong resemblance to that of a typical spin glass system. Thus, we may conclude that the transition to these states in the thermodynamic limit corresponds to a glassy freezing transition.

We note that an observation that for sufficiently long sequences of alternating monomers (“short” blocks) the micro-phase separated state is displaced by the region of glassy frustrated phases has been known for quite some time and well understood in the framework of the density theories [9] as a result of the density fluctuations which modify the mean-field behaviour. The block translational symmetry breaking in our approach is another manifestation of the glassy phenomena earlier extensively studied for melts of random heteropolymers. In addition, we can see how the destruction of the micro-phase structures occurs for finite-sized systems and how exactly it depends on a particular sequence.

The folding kinetics is found to be strongly affected by the presence of these transient frustrated states along the kinetic pathway. This leads to a complicated kinetic process consisting of multiple steps with pronounced slowing down and then acceleration in the folding rate. It is interesting to note that a typical fairly heterogeneous chain with weakly hydrophilic and strongly hydrophobic units folds kinetically first to one of the misfolded states and can undergo a consequent nucleation process to the main thermodynamic state of the micro-phase separated globule.

These results for equilibrium and kinetics confirm many predictions of the earlier treatment adopted for random heteropolymers in Ref. [12] based on a quasi-perturbative averaging of the GSC equations over the quenched disorder. The latter approach describes a large set of random heteropolymer sequences with a Gaussian distribution of the monomer amphiphilicity. The kinetics of folding seems to be consistent between the previous and current approaches with respect to main observables such as the radius of gyration, energy and the MPS parameter. A smooth slow glass-like relaxation in the former approach is produced by averaging over all different sequences with their particular multistep processes of passage through the frustrated states. Although here we observe strong dependence of the phase

boundaries in the equilibrium phase diagram on the primary sequence, the major conclusion of Refs. [12,13] that there are three distinct globular states of the homopolymer-like (liquid), the frozen (glassy) and the micro-phase separated (folded) globules, and an additional state of the random coil, as well their relative location in the diagram, remain valid. We have previously discussed that the equilibrium limit of the theory in the treatment of Ref. [13] had certain deficiencies due to the additional perturbative approximation, which we attempted to remedy phenomenologically. The current fundamental scheme is free of any such problems and provides a reliable test ground for development of further approximations.

We have also discovered that heteropolymer sequences of equal length can be roughly divided into distinct classes possessing similar phase diagrams and kinetic folding properties. For instance, periodic polymers with a few long blocks easily undergo micro-phase separation and for them the frustrated states are suppressed at equilibrium and in kinetics. There is a view in the scientific community that complex random sequences also permit more refined classification. The identification of good folding sequences (see e.g. Ref. [28]) is believed to be an important prerequisite for unraveling the mysteries of proteins.

In the current paper the GSC method has been applied to a single chain problem. However, since the kinetic equations (17) are covariant it would be relatively straightforward to apply it to solutions of many polymers. Formation of nontrivial mesoscopic globules in copolymer solutions at low concentrations has been predicted in the framework of the method [29] and recently observed experimentally [30]. Generally, the GSC method may be viewed as extension to the realm of kinetics of the variational treatment, which is a better theory than standard mean-field approaches due to a much larger number of variational parameters. We should admit, however, that in the complete form numerical solution of the GSC equations is computationally expensive for systems of a few hundred of monomers. Nevertheless, as we have recently shown [29], in some approximation the GSC equations can be reduced to those of a simple mean-field theory such as the Flory-Huggins one, and some extra corrections to the latter. Importantly, the formalism in terms of the mean-squared distances is valid for description of the extended coil as well as of the globular states, whereas the density formalism theories are limited to relatively high densities of the system. The weakest point of the method is the Gaussian form of the trial Hamiltonian, and thus of the correlation functions, a matter that has been discussed at some length in the past [25,14]. However, based on the covariant form of the kinetic equations derived here, we hope, in some not too distant future, to take into account the non-Gaussian corrections in an analogy to the treatment of the hard-core repulsion for van der Waals systems.

The main strength of the revised GSC approach lies in the ability to describe a given heteropolymer sequence of finite length, rather than an *infinite ensemble* of sequences characterised in a certain probabilistic way. This is an inevitable preliminary step in developing adequate techniques for theoretical modelling of complex biopolymers. Understanding of the relation between the chemical composition (primary sequence) and the 3-d equilibrium (tertiary) structure, as well as of the kinetics of folding, in proteins is one of the great challenges of the modern biotechnological science. We hope that methods like the one we have presented here will take their right place in the collection of new tools for bioinformatics.

ACKNOWLEDGMENTS

The authors acknowledge interesting discussions with Professor C.A. Angell, Professor K. Kawasaki, Professor G. Parisi, and our colleagues Dr A.V. Gorelov and A. Moskalenko.

APPENDIX A: INCLUSION OF HYDRODYNAMICS

The Langevin equation with account of the hydrodynamic interaction includes the Oseen tensor [4],

$$\frac{d}{dt}X_n^\alpha = \sum_{\alpha', n'} H_{nn'}^{\alpha\alpha'}[X(t)] \phi_{n'}^{\alpha'}, \quad (\text{A1})$$

where ϕ_n^α is the right-hand side of Eq. (1) and the noise has the second momentum proportional to the inverse Oseen tensor.

In the preaveraged approximation we have,

$$\langle H_{mm'}^{\alpha\alpha'} \rangle = \delta^{\alpha\alpha'} \xi_{mm'}, \quad \xi_{mm'} = \frac{\delta_{mm'}}{\zeta_b} + \frac{1 - \delta_{mm'}}{3(2\pi^3)^{1/2} \eta_s D_{mm'}^{1/2}}, \quad (\text{A2})$$

and the analogs of formulae (A5,A6) of Ref. [11] will be,

$$\frac{1}{2} \frac{d}{dt} D_{nn'} = \sum_{m'} (\xi_{nm'} - \xi_{n'm'}) (\Gamma_{nm'} - \Gamma_{n'm'}), \quad (\text{A3})$$

$$\Gamma_{nn'} = -\frac{2}{3} \sum_{m''} D_{nm''} \frac{\partial \mathcal{A}}{\partial D_{n'm''}} = k_B T \delta_{nn'} + \sum_{m''} D_{nm''} V_{n'm''}. \quad (\text{A4})$$

Explicit expressions for a few first terms in the virial expansion of the effective potentials,

$$V_{mm'} = -\frac{2}{3} \frac{\partial \mathcal{E}}{\partial D_{mm'}} \quad (\text{A5})$$

may be found in Appendix C.

APPENDIX B: THE VARIATIONAL PRINCIPLE

We introduce the trace as the integration over all monomers coordinates subject to the constraint that the reference point is fixed in the centre-of-mass of the chain,

$$\text{Tr} \equiv \int \prod_{n=0}^{N-1} d\mathbf{X}_n \delta\left(\sum_n \mathbf{X}_n\right). \quad (\text{B1})$$

Then the partition function is obtained as $Z_{tot} = \text{Tr} \exp(-H/k_B T)$ with H given by Eq. (3). The delta-function in (B1) removes the trivial divergence in Z_{tot} due to the translational invariance.

We choose the trial Hamiltonian as an arbitrary linear combination,

$$\frac{H_0}{k_B T} = \frac{1}{2} \sum_{mm'} K_{mm'} \mathbf{X}_m \mathbf{X}_{m'} + \sum_m \mathbf{J}_m \mathbf{X}_m, \quad (\text{B2})$$

where we have also introduced arbitrary sources \mathbf{J}_m . Using the delta-function one can exclude, say, \mathbf{X}_0 and derive,

$$Z_0[J] = (2\pi)^{3(N-1)/2} (\det \tilde{K}^{(N-1)})^{-3/2} \exp\left(\frac{1}{2} \sum_{mm'} '(\mathbf{J}_m - \mathbf{J}_0)(\tilde{K}^{-1})_{mm'}(\mathbf{J}_{m'} - \mathbf{J}_0)\right), \quad (\text{B3})$$

where the $N-1$ dimensional matrix \tilde{K} is

$$(\tilde{K})_{nn'} = K_{nn'} + K_{00} - K_{n0} - K_{0n'}. \quad (\text{B4})$$

We can calculate the averages by,

$$\mathcal{F}_{nn'} = \frac{1}{3} \langle \mathbf{X}_n \mathbf{X}_{n'} \rangle_0 = \frac{1}{3} \frac{\partial^2 \log Z_0[J]}{\partial \mathbf{J}_n \partial \mathbf{J}_{n'}} = (\tilde{K}^{-1})_{nn'}, \quad (\text{B5})$$

where again the latter identity holds only for $n, n' \neq 0$. From these quantities it is straightforward to obtain the mean squared distances using Eq. (6) which also holds only for $n, n' \neq 0$.

Finally, we want to express all independent parameters of the matrix \tilde{K} via the quantities $D_{mm'}$. For this we compute the following sums applying the above delta-function constraint,

$$\sum_{mm'} D_{mm'} = 2N \sum_m \mathcal{F}_{mm}, \quad \sum_m D_{mn} = \frac{1}{2N} \sum_{mm'} D_{mm'} + N \mathcal{F}_{nn}. \quad (\text{B6})$$

Substituting \mathcal{F}_{nn} from the second formula here to Eq. (12) and recalling the relation (8) we derive the desired inverse relation (12) for $(\tilde{K}^{-1})_{nn'} = \mathcal{F}_{nn'}$.

From the partition function (B3) we obtain the “entropic” term $\mathcal{A}_0 \equiv -T\mathcal{S} = -k_B T \log Z_0[0]$ that yields precisely Eq. (11). The Gibbs–Bogoliubov variational principle is then based on minimising this variational free energy $\mathcal{A} = \mathcal{A}_0 + \langle H - H_0 \rangle_0$ with respect to the $N(N-1)/2$ independent variational parameters $D_{mm'}$.

1. Entropy of the homopolymer

For the homopolymer we have the translational invariance along the chain so that $D_{nn'} = D_k$, where $k = |n - n'|$. Then the matrix (12) may be rewritten as,

$$R_{nn'} = R_g^2 - \frac{1}{2}D_{nn'}, \quad R_g^2 = \frac{1}{2N} \sum_k D_k. \quad (\text{B7})$$

Let us apply a unitary transformation to the Fourier coordinates generated by the matrix,

$$f_n^q = \frac{1}{N^{1/2}} \exp\left(-\frac{2\pi i q n}{N}\right). \quad (\text{B8})$$

By a direct evaluation and recalling the relation for the normal modes,

$$-\frac{1}{2N^{1/2}} \sum_k \text{Re } f_k^q D_k = \mathcal{F}_q, \quad (\text{B9})$$

we see that the matrix $\tilde{R} = f^\dagger \bullet R \bullet f$ is diagonal with the eigenvalues $\tilde{R}_{00} = 0$ and $\tilde{R}_{qq} = N\mathcal{F}_q$. Thus, the logarithm of determinant of the $(N - 1)$ -dimensional submatrix $\det' \tilde{R}$ yields the standard “entropy” of the homopolymer (see Eq. (3) in Ref. [17]) up to a trivial constant.

APPENDIX C: FORMULAE FOR THE EFFECTIVE POTENTIALS

Two first terms in the virial expansion of the derivatives (A5) of the mean energy are explicitly given by,

$$V_{mm'}^{(2)} = (1 - \delta_{mm'}) \frac{\hat{u}_{mm'}^{(2)}}{D_{mm'}^{5/2}} - \delta_{mm'} \sum_{\substack{n \\ n \neq m}} \frac{\hat{u}_{mn}^{(2)}}{D_{mn}^{5/2}}, \quad (\text{C1})$$

$$V_{mm'}^{(3)} = (1 - \delta_{mm'}) 3\hat{u}^{(3)} \sum_{\substack{n \\ n \neq m, m'}} \frac{D_{mn, m'n}}{(\det \Delta^{(2)})_{mm'n}^{5/2}} - \delta_{mm'} \frac{3}{2} \hat{u}^{(3)} \sum_{\substack{n, n' \\ n \neq n' \neq m}} \frac{D_{nn'}}{(\det \Delta^{(2)})_{mnn'}^{5/2}}, \quad (\text{C2})$$

where $(\det \Delta^{(2)})_{mm'm''} = D_{mm'} D_{m''m'} - D_{mm'', m'm'}^2$.

It is usually assumed that for negative $\bar{u}^{(2)}$ the stability of the system is ensured by the positiveness of $u^{(3)}$. It turns out however that for the whole range of $u_{mm'}^{(2)}$ this does not hold and there are additional pathological solutions with singular free energy. The reason for this deficiency of the model (3) is that we have discarded the terms with two coinciding indices in the three-body contribution. This standard trick is not satisfactory therefore, but fortunately it could be remedied by using another prescription for these terms:

$$\mathcal{E}_3 = u^{(3)} \sum_{m \neq m' \neq m''} \left\langle \delta(\mathbf{X}_m - \mathbf{X}_{m'}) \delta(\mathbf{X}_{m''} - \mathbf{X}_{m'}) \right\rangle + 3u^{(3)} \sum_{m \neq m'} \left\langle \delta(\mathbf{X}_m - \mathbf{X}_{m'}) \right\rangle^2. \quad (\text{C3})$$

In Ref. [31] we show that the addition of the latter term, which is subdominant in the large N limit anyway, does not change the earlier results for the homopolymer, and even quantitatively improves the agreement with known results for the dense globular state [5]. Importantly, for heteropolymers this term removes spurious solutions and makes the theory well defined. The corresponding contributions to the mean energy and the effective potentials are,

$$\mathcal{E}^{(3')} = 3\hat{u}^{(3)} \sum_{m \neq m'} D_{mm'}^{-3}, \quad V^{(3')} = (1 - \delta_{mm'}) 6\hat{u}^{(3)} D_{mm'}^{-4} - \delta_{mm'} 6\hat{u}^{(3)} \sum_{\substack{n \\ n \neq m}} D_{mn}^{-4}. \quad (\text{C4})$$

- [1] M. L. Huggins, J. Chem. Phys. **9**, 440 (1941); P. J. Flory, J. Chem. Phys. **9**, 660 (1941); *Polymer Blends*, edited by D. R. Paul and S. Neuman (Academic Press, 1987); *Multicomponent Polymer Systems*, edited by I. S. Miles and S. Rostami (Longman Scientific and Technical, Singapore, 1992).
- [2] P. G. de Gennes, *Scaling Concepts in Polymer Physics* (Cornell University Press, Ithaca, NY, 3rd printing, 1988).
- [3] J. des Cloizeaux and G. Jannink, *Polymers in Solution* (Clarendon Press, Oxford, 1990).
- [4] M. Doi and S. F. Edwards, *The Theory of Polymer Dynamics* (Oxford Science, New York, 1989).
- [5] A. Yu. Grosberg and A. R. Khokhlov, *Statistical Physics of Macromolecules* (AIP, NY, 1994).
- [6] D. J. Meier, J. Polym. Sci. **C26**, 81 (1969); D. J. Meier, J. Polym. Prepr. **11**, 400 (1970); **15**, 171 (1974); A. N. Semenov, Sov. Phys. JETP **61**, 733 (1985); T. Ohta and K. Kawasaki, Macromolecules **19**, 2621 (1986); L. Leibler, Macromolecules **13**, 1602 (1980); G. H. Fredrickson and E. Helfand, J. Chem. Phys. **87**, 697 (1987); T. Hashimoto, Macromolecules **20**, 465 (1987).
- [7] G. H. Fredrickson, S. T. Milner, and L. Leibler, Macromolecules **25**, 6341 (1992).
- [8] T. Garel and H. Orland, Europhys. Lett. **6** (4), 307 (1988); **6**, 597 (1988).
- [9] E. I. Shakhnovich and A. M. Gutin, J. Phys. (France) **50** 1843, (1989); S. V. Panyukov and S. I. Kuchanov, Sov. Phys. JETP **72** (2), 368 (1991); A. V. Dobrynin and I. Ya. Erukhimovich, Pis'ma Zh. Eksp. Teor. Fiz. **53** (11) 545 (1991), J. Phys. **I** **5** 365 (1995).
- [10] P. G. Wolynes, in *Spin glass ideas in biology*, edited by D. Stein (World Scientific, Singapore, 1991); *Protein Folding*, edited by T. E. Creighton (Wiley, New York, 1992); *New Developments in Theoretical Studies of Proteins*, edited by R. Elber (World Scientific, Singapore, 1994).
- [11] E. G. Timoshenko, Yu. A. Kuznetsov, and K. A. Dawson, Phys. Rev. E **53** (4), 3886 (1996).
- [12] E. G. Timoshenko, Yu. A. Kuznetsov, and K. A. Dawson, Phys. Rev. E **54** (4), 4071 (1996).
- [13] E. G. Timoshenko, Yu. A. Kuznetsov, and K. A. Dawson, Phys. Rev. E **55** (5), 5750 (1997).
- [14] Yu. A. Kuznetsov, E. G. Timoshenko, and K. A. Dawson, J. Chem. Phys. **104** (9), 3338 (1996).
- [15] This is accomplished by integrating out its degrees of freedom from the path integral representation for the partition function [13].
- [16] O. Kratky and G. Porod, Rec. Trav. Chim. **68**, 1106 (1949).
- [17] Yu. A. Kuznetsov, E. G. Timoshenko, and K. A. Dawson, J. Chem. Phys. **105**(16), 7116 (1996).
- [18] Note that one may use the symmetry properties $D_{mm'} = D_{m'm}$ and $D_{mm} = 0$ only after the differentiation of the energy (10), which is generally speaking expressed through the four-point correlation functions. One should use the standard differentiation rule, $\partial D_{kk'}/\partial D_{mm'} \equiv \delta_m^k \delta_{m'}^{k'}$. The structure of the kinetic equations is such that the symmetry properties are automatically satisfied on the solution of these equations at each moment in time.
- [19] Yu. A. Kuznetsov, E. G. Timoshenko, and K. A. Dawson, submitted to Physica A (1998)..
- [20] W. H. Press, S. A. Teukolsky, W. T. Vetterling, and B. P. Flannery, *Numerical Recipes in C* (Cambridge University Press, 1992).
- [21] Apparently, for a finite length chain, the collapse transition is characterised by a finite width, and therefore its representation in Figs. 1-3 is sufficiently schematic with a suitable criterion [17] adopted to draw a definite curve for it.
- [22] The curve (S) in Figs. 1-3 is defined by the condition $\Psi = 1/2$, i.e. half of maximal possible value of the MPS parameter.
- [23] Yu. A. Kuznetsov, E. G. Timoshenko, and K. A. Dawson, J. Chem. Phys. **103**(11), 4807 (1995).
- [24] M. Mezard, G. Parisi, and M. Virasoro, *Spin glass theory and beyond* (World Scientific, Singapore, 1987).
- [25] E. G. Timoshenko, Yu. A. Kuznetsov, and K. A. Dawson, J. Chem. Phys. **102** (4), 1816 (1995).
- [26] P. G. Wolynes, J. N. Onuchic, and D. Thirumalai, Science **267**, 1619 (1995).
- [27] G. Parisi, in *Proceedings of the International Conference on Morphology and Kinetics of Phase Separating Complex Fluids*, edited by F. Mallamace (Messina, Italy, 1997).
- [28] A. Irbäck, C. Peterson, and F. Potthast, Phys. Rev. E **55**, 4260 (1997).
- [29] E. G. Timoshenko, Yu. A. Kuznetsov, and K. A. Dawson, Physica A **240** 432 (1997); Proceedings of the International Conference on Morphology and Kinetics of Phase Separating Complex Fluids, ed. by F. Mallamace (Messina, Italy, 1997).
- [30] A. V. Gorelov, A. du Chesne, and K. A. Dawson, Physica A **240**, 443 (1997); X. Qiu, C. M. S. Kwan, and C. Wu, Macromolecules **30** 6090 (1997).
- [31] Yu. A. Kuznetsov, E. G. Timoshenko, and K. A. Dawson, in *Proceedings of the International Conference on Morphology and Kinetics of Phase Separating Complex Fluids*, edited by F. Mallamace (Messina, Italy, 1997), to be published in Il Nuovo Cimento.

FIG. 1. The phase diagram of copolymer sequence 30(ab) (“short” blocks) in terms of the mean second virial coefficient, $\bar{u}^{(2)}$, and the amphiphilicity, Δ (both in units $k_B T \mathcal{L}^3$). Curves (C) and (S) correspond respectively to the collapse and the micro-phase separation continuous transitions. Curves (I) and (II) correspond to discontinuous transitions to the frustrated phases. “Spinodal” curves (I’) and (II’) bound the regions of metastability of the frustrated states. Transition curves and boundaries distinguishing different frustrated states are not depicted.

FIG. 2. The phase diagram of copolymer sequence 10(aaabbb) (“long” blocks) in terms of the mean second virial coefficient, $\bar{u}^{(2)}$, and the amphiphilicity, Δ (both in units $k_B T \mathcal{L}^3$). For large values of Δ the collapse transition becomes discontinuous (curve (I)) and it is accompanied by micro-phase separation (see also Figs. 7-8). Curves (I') and (I'') are spinodals.

FIG. 3. The phase diagram of the “random” sequence 2(abacbbcabccbbcaaacbccbbaacbcc) in terms of the mean second virial coefficient, $\bar{u}^{(2)}$, and the amphiphilicity, Δ (both in units $k_B T \mathcal{L}^3$). Other notations are as in Fig. 1.

FIG. 4. Diagrams of the mean squared distances matrix $D_{mm'}$ for the “short” blocks copolymer 30(ab) at $\Delta = 20$. Diagrams (a-d) correspond respectively to $u^{(2)} = 15, -21, -30$ and -40 (in units $k_B T \mathcal{L}^3$). Indices m, m' start counting from the upper left corner. Each matrix element, $D_{mm'}$ is denoted by a quadratic cell with varying degree of black colour, the darkest and the lightest cells corresponding respectively to the smallest and to the largest mean squared distances. The diagonal elements are not painted since $D_{mm} = 0$. For the coil (Fig. a) $D_{mm'}$ elements increase monotonically on moving away from the diagonal towards half-ring distance along the chain. In frustrated states (Figs. b,c) $D_{mm'}$ possesses some number of clusters with monomers having smaller distances between each other. For the MPS globule (Fig. d) $D_{mm'}$ reflects the structure of the two-body interaction matrix $u_{mm'}^{(2)}$ and consists of similar elementary cells.

FIG. 5. Plot of the mean squared radius of gyration, R_g^2 (in units \mathcal{L}^2), vs the amphiphilicity, Δ (in units $k_B T \mathcal{L}^3$), for different sequences (from top to bottom): “long” blocks, “short” blocks and the “random” sequence. Here we have fixed $\bar{u}^{(2)} = -40$.

FIG. 6. Plot of the parameter of micro-phase separation, Ψ , vs the amphiphilicity, Δ (in units $k_B T \mathcal{L}^3$), for different sequences: “long” blocks (pluses), “short” blocks (diamonds) and the “random” sequence (quadrangles). Here we have fixed $\bar{u}^{(2)} = -40$.

FIG. 7. Plot of the mean squared radius of gyration, R_g^2 (in units \mathcal{L}^2), vs the second virial coefficient, $\bar{u}^{(2)}$ (in units $k_B T \mathcal{L}^3$), for 10(aaabbb) copolymer. Here and in Figs. 8-10 $\Delta = 30$, solid lines correspond to values of observables in the main free energy minimum and dashed lines — in the metastable minima.

FIG. 8. Plot of the parameter of micro-phase separation, Ψ , vs the second virial coefficient, $\bar{u}^{(2)}$ (in units $k_B T \mathcal{L}^3$), for 10(aaabbb) copolymer.

FIG. 9. Plot of the mean squared radius of gyration, R_g^2 (in units \mathcal{L}^2), vs the second virial coefficient, $\bar{u}^{(2)}$ (in units $k_B T \mathcal{L}^3$), for the “random” sequence.

FIG. 10. Plot of the parameter of micro-phase separation, Ψ , vs the second virial coefficient, $\bar{u}^{(2)}$ (in units $k_B T \mathcal{L}^3$), for the “random” sequence.

FIG. 11. Time evolution (t is in units \mathcal{T}) of the mean squared radius of gyration, R_g^2 (in units \mathcal{L}^2), for different sequences after an instantaneous quench from the coil state, $\bar{u}^{(2)} = 15$ and $\Delta = 0$, to the region with $\bar{u}^{(2)} = -25$ and $\Delta = 30$.

FIG. 12. Time evolution (t is in units \mathcal{T}) of the parameter of micro-phase separation, Ψ , for different sequences after the same quench as in Fig. 11.

FIG. 13. Time evolution (t is in units \mathcal{T}) of the instantaneous free energy, \mathcal{A} (in units $k_B T$), for different sequences after the same quench as in Fig. 11.

FIG. 14. Time evolution (t is in units \mathcal{T}) of the mean squared distances between nearest ‘a’ monomers $D_{2k,2k+2}(t)$ (in units \mathcal{L}^2) for 30(ab) copolymer in kinetics after the quench with the final two-body parameters: $\bar{u}^{(2)} = -50$ and $\Delta = 30$.

FIG. 15. Diagrams of $D_{mm'}(t)$ matrix for the “short” blocks copolymer 30(ab) in kinetics after the same quench as in Fig. 14. Diagrams (a-c) correspond respectively to the following moments in time: $t = 4.6$, 11, and 12.9. See also caption to Fig. 4 for more details. The kinetic process proceeds through formation of locally collapsed and phase-separated clusters. The initial conformation is similar to Fig. 4a, then some clusters appear, coalesce into larger ones, until they eventually unify forming the MPS globule (similar to Fig. 4d).

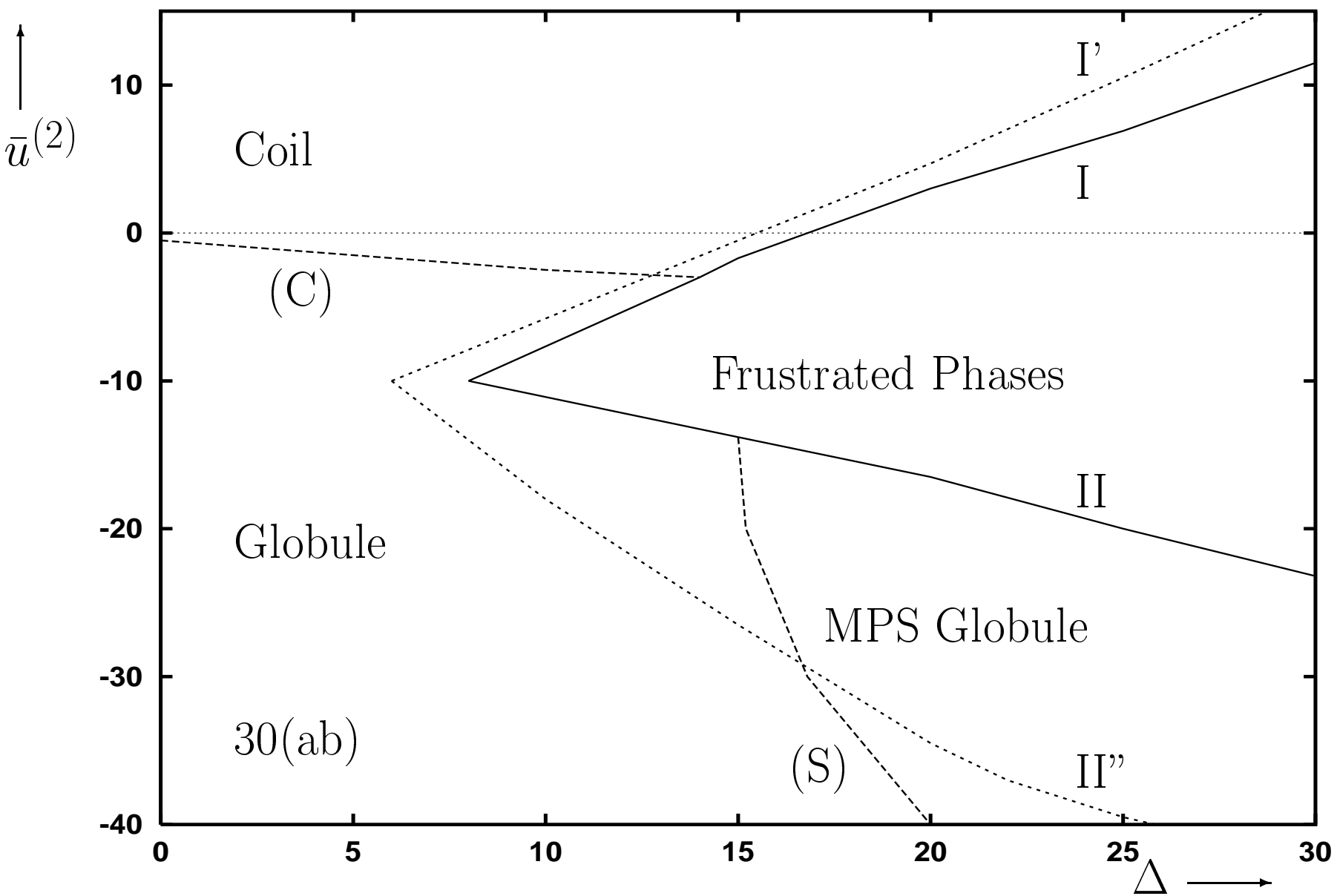


Fig. 1

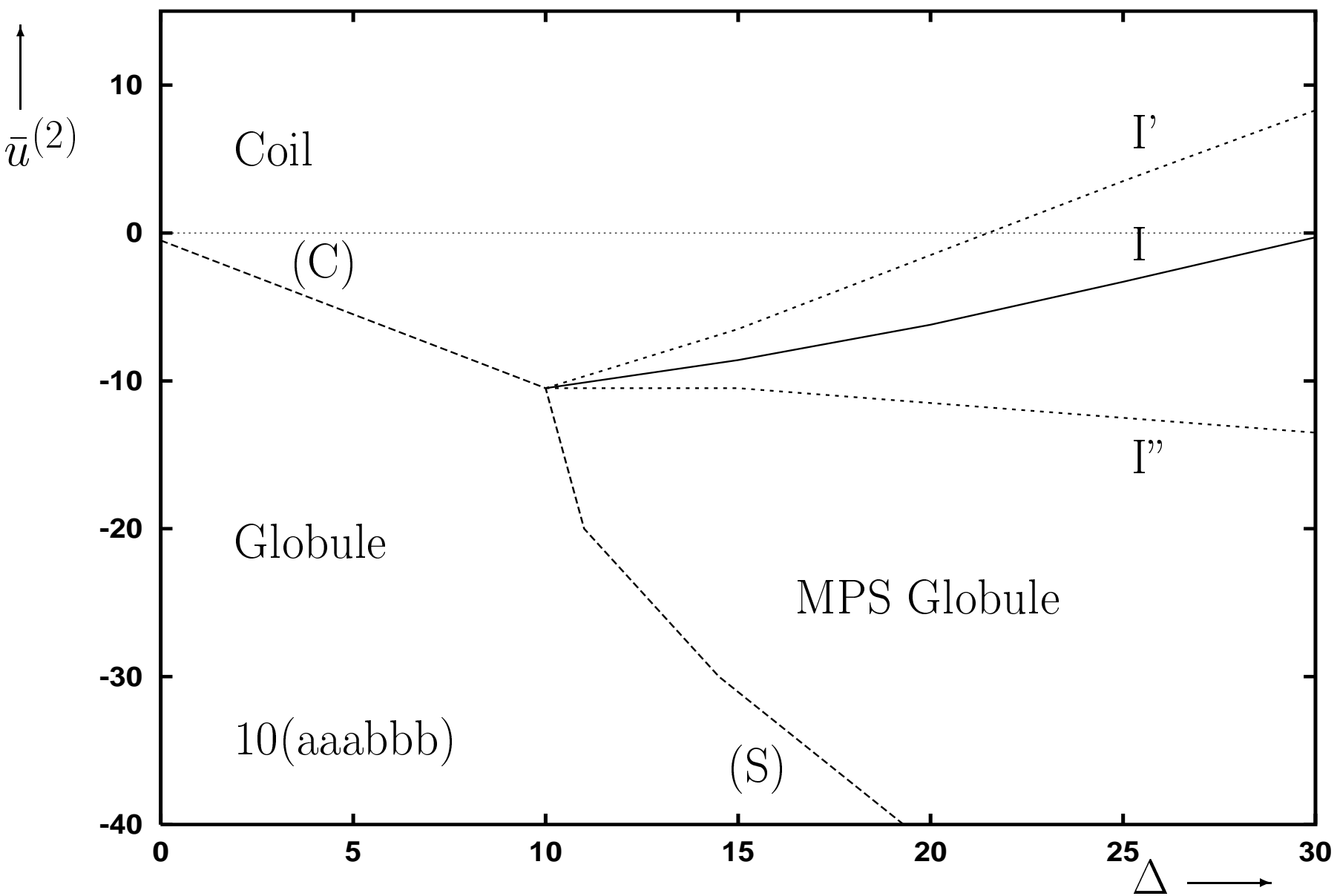


Fig. 2

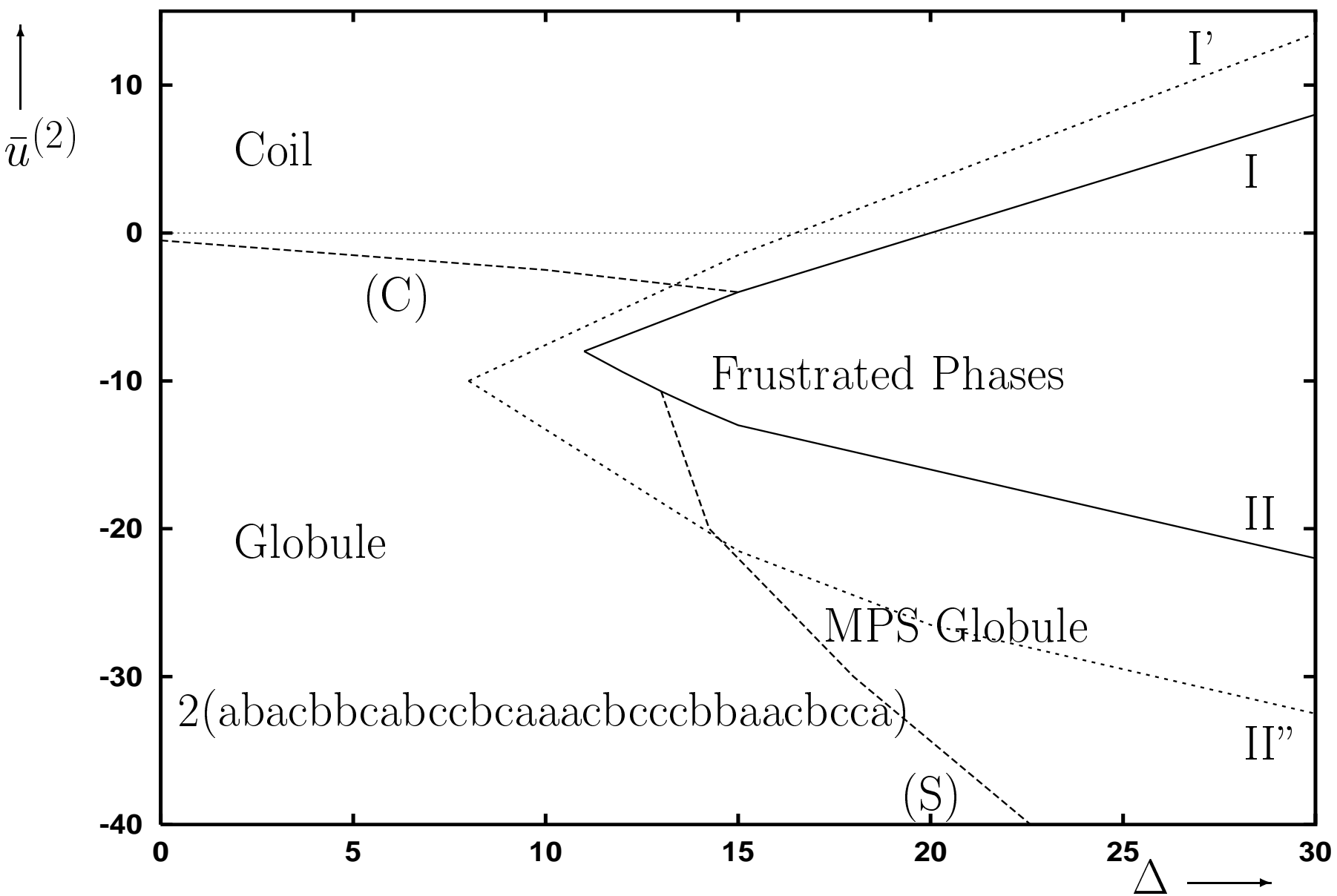


Fig. 3

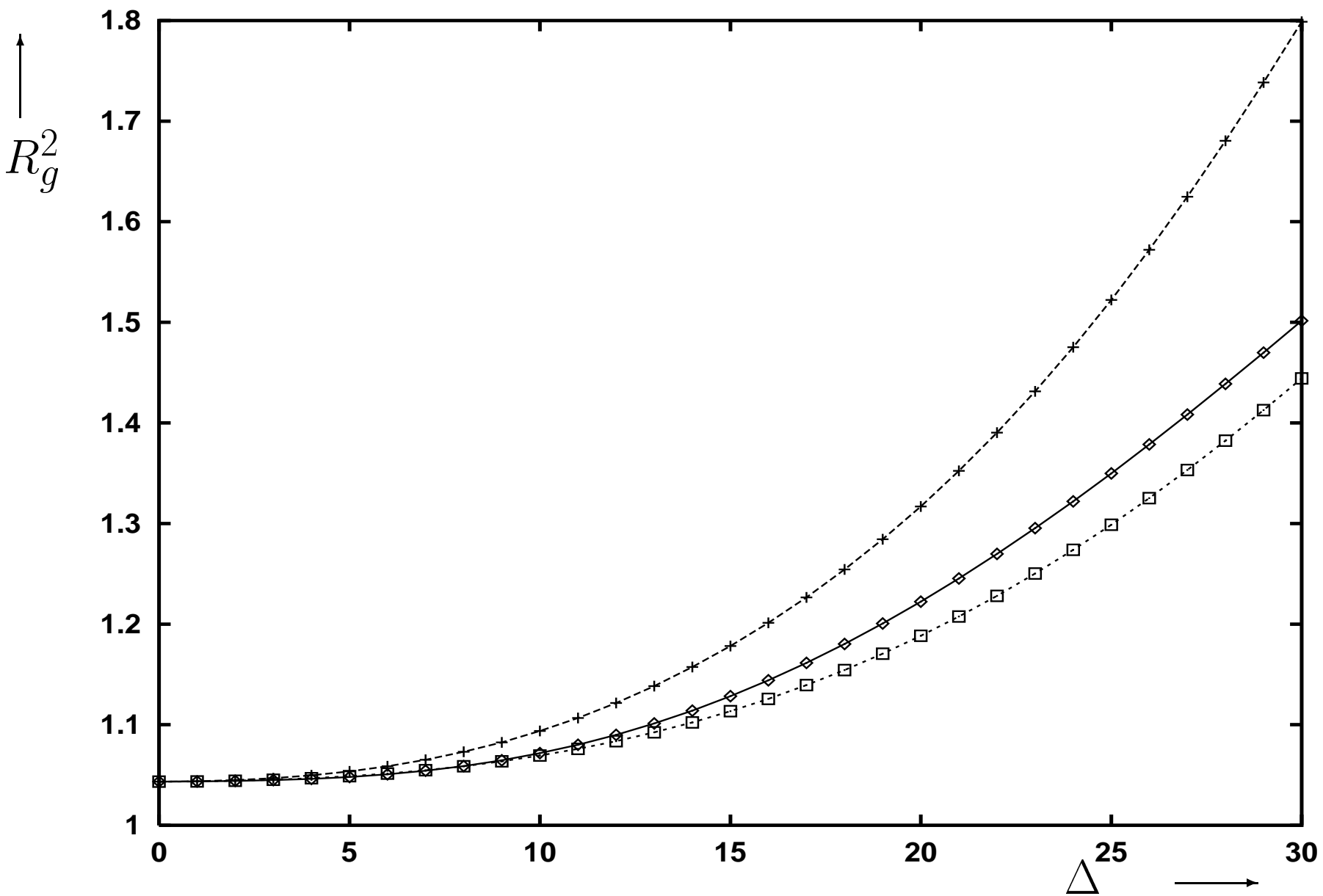


Fig. 5

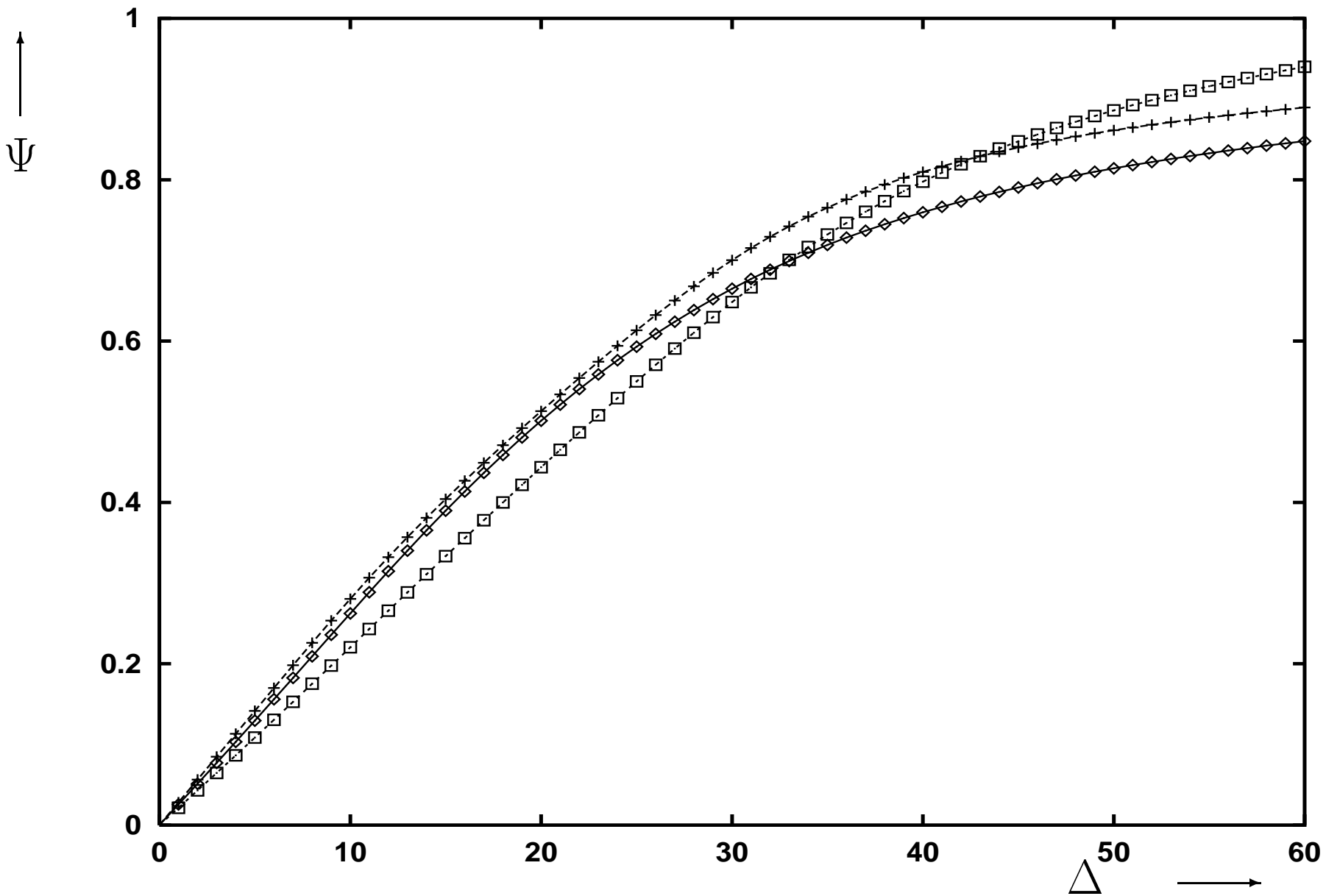


Fig. 6

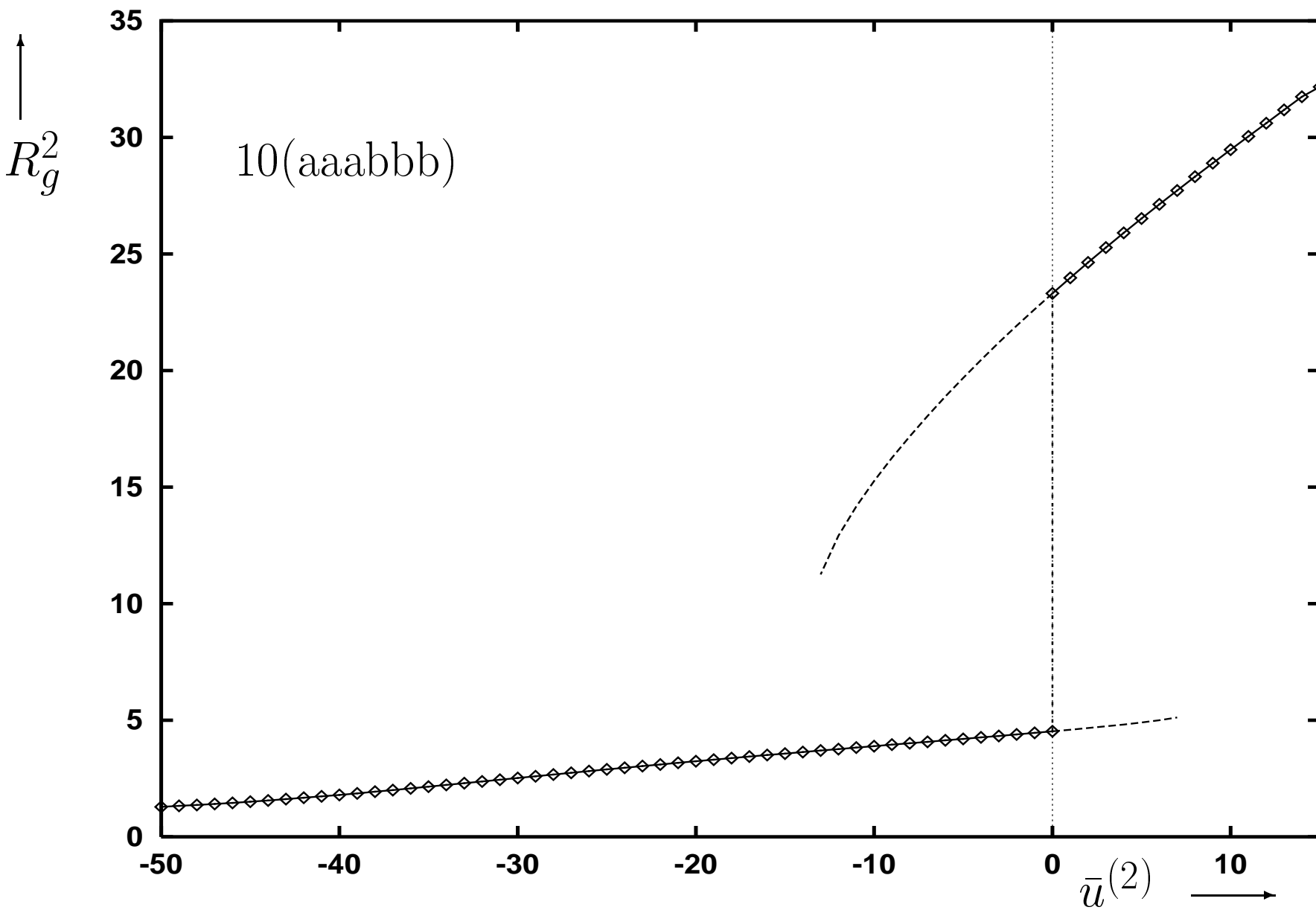


Fig. 7

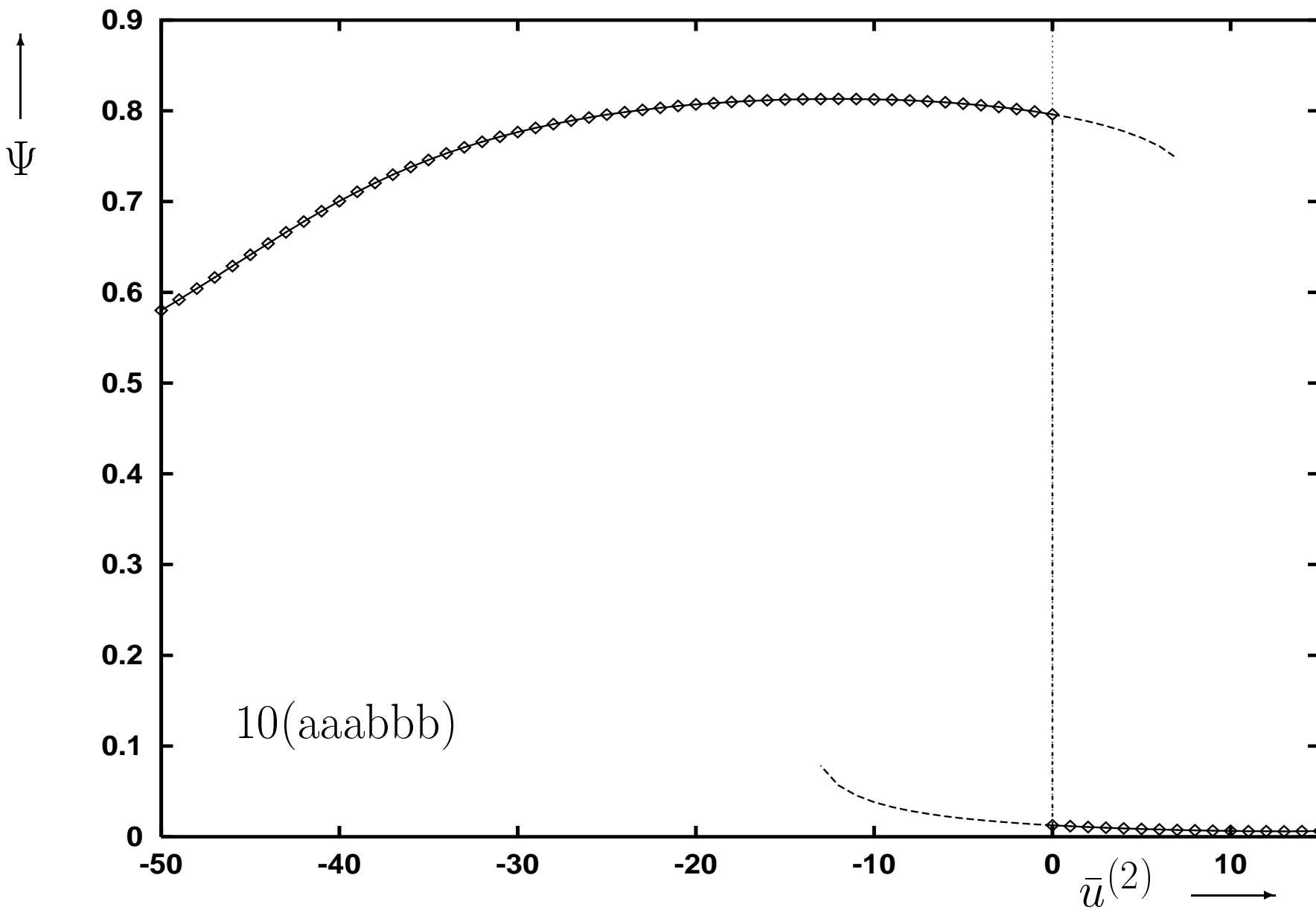


Fig. 8

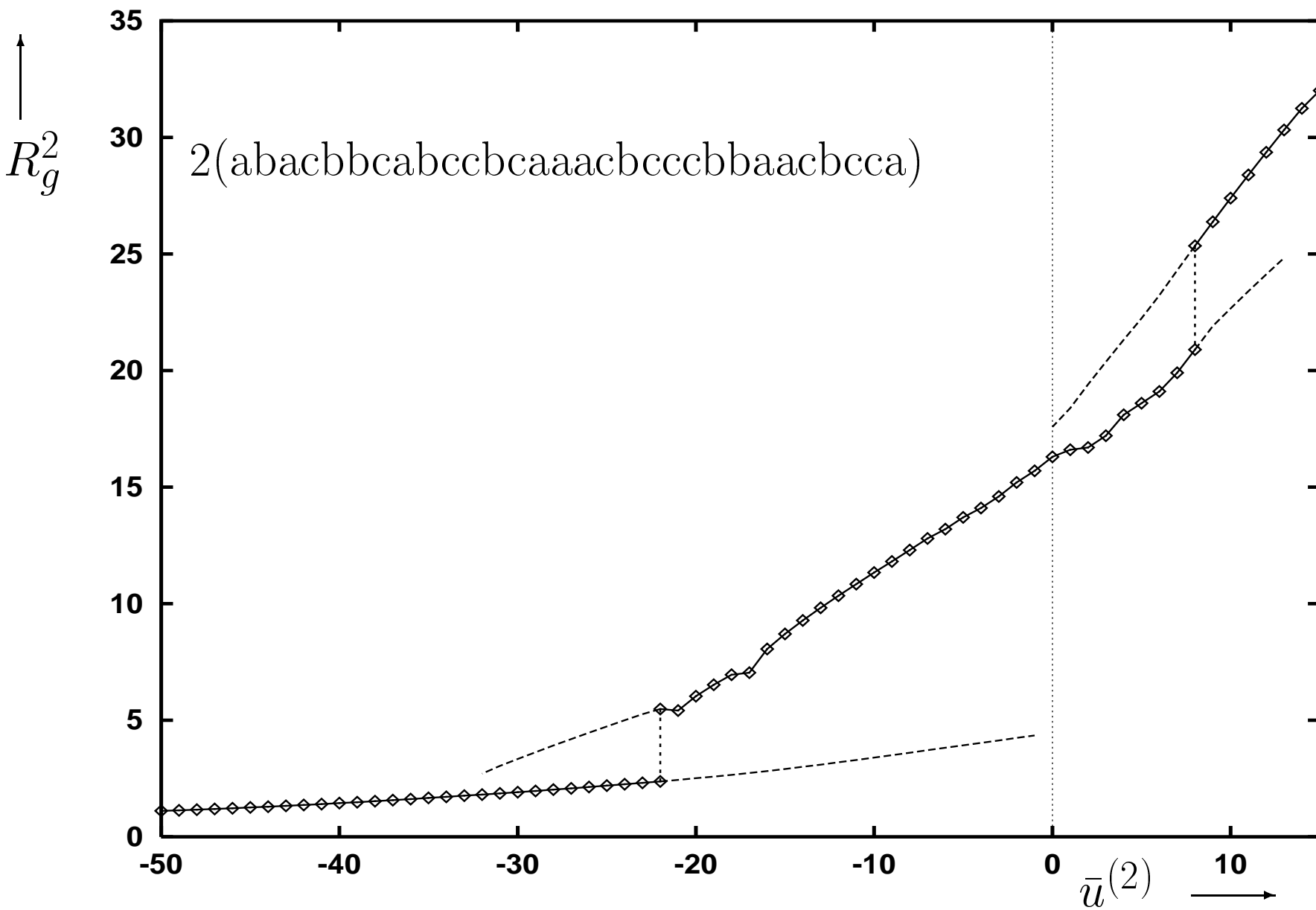


Fig. 9

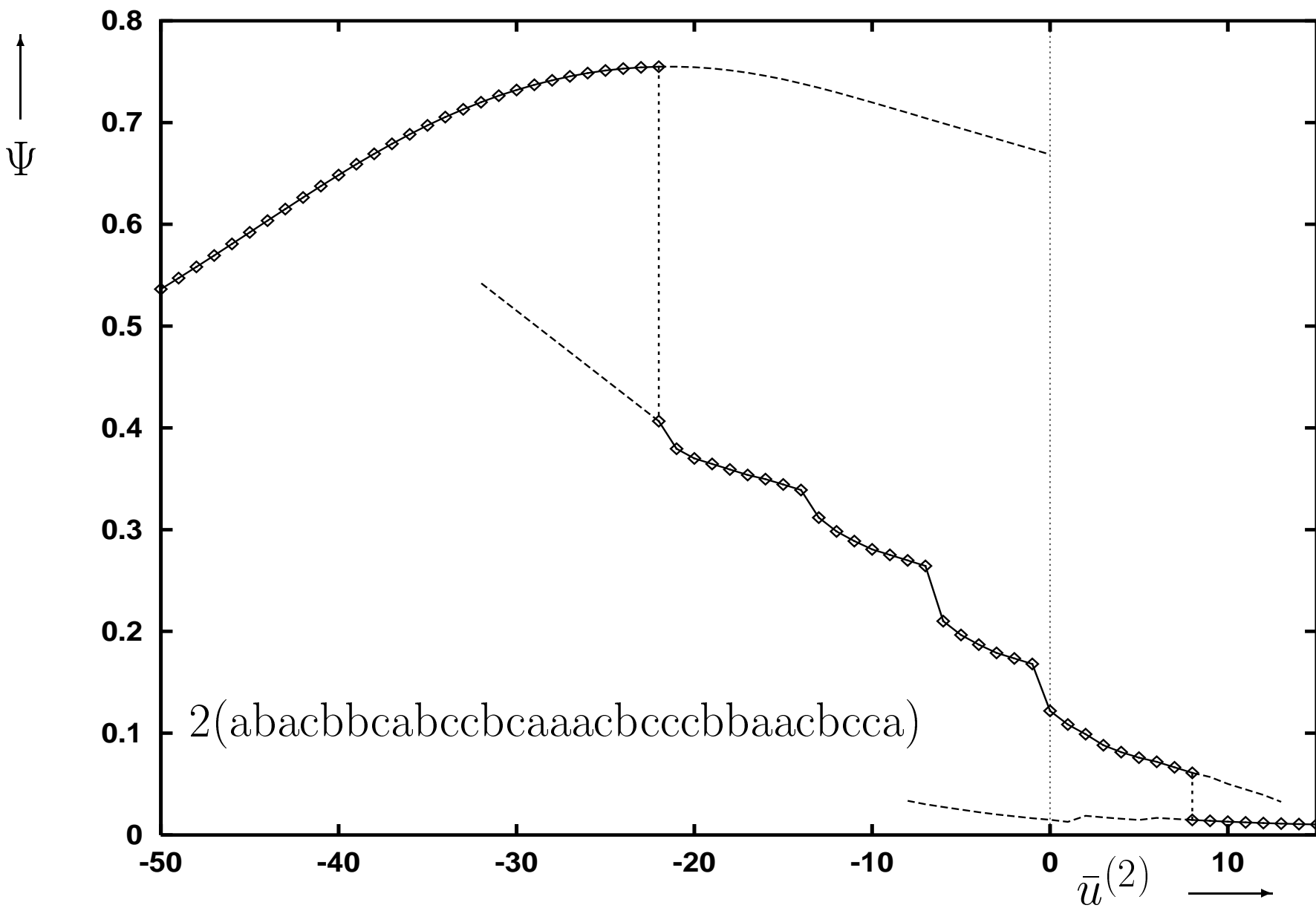


Fig. 10

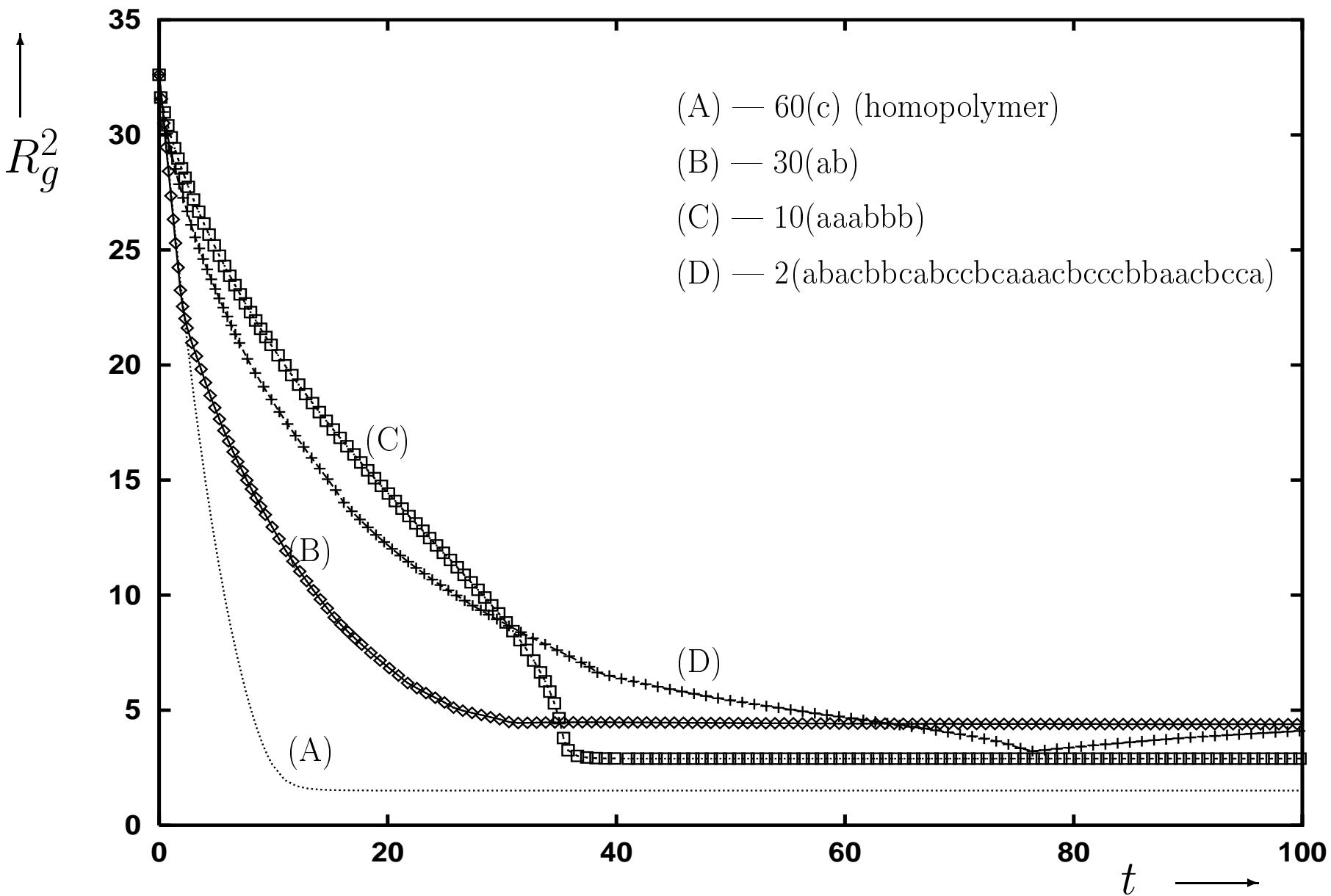


Fig. 11

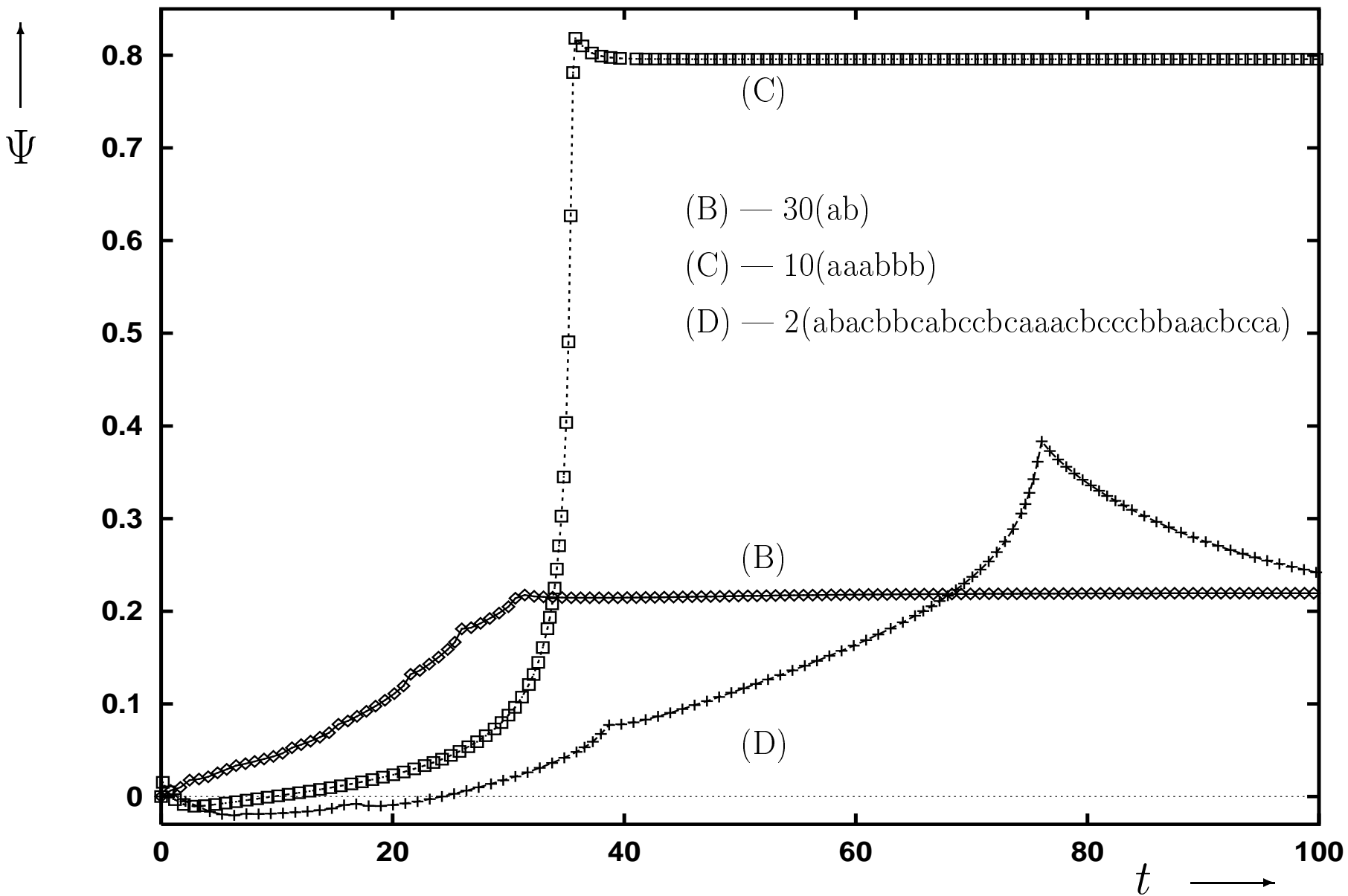


Fig. 12

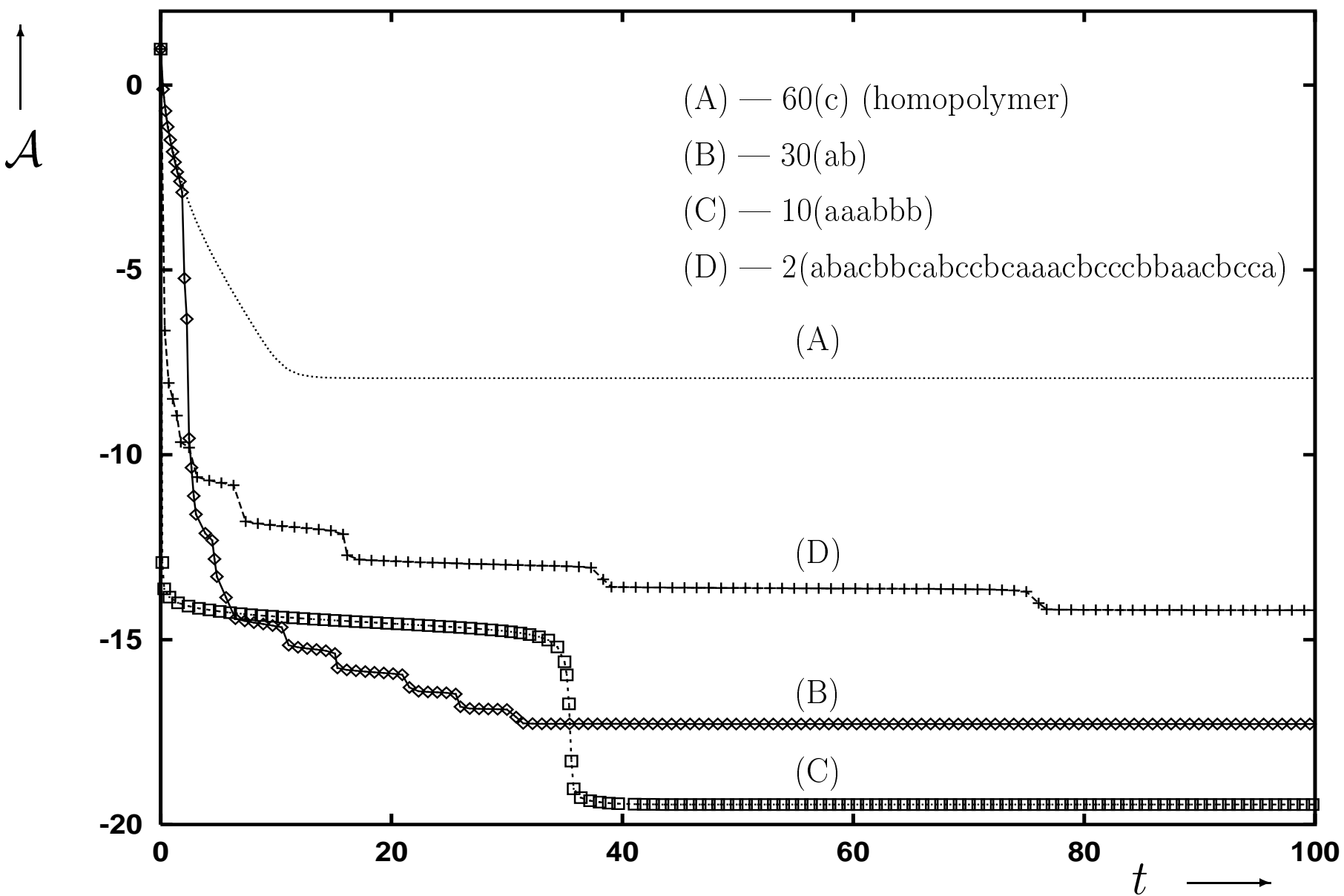


Fig. 13

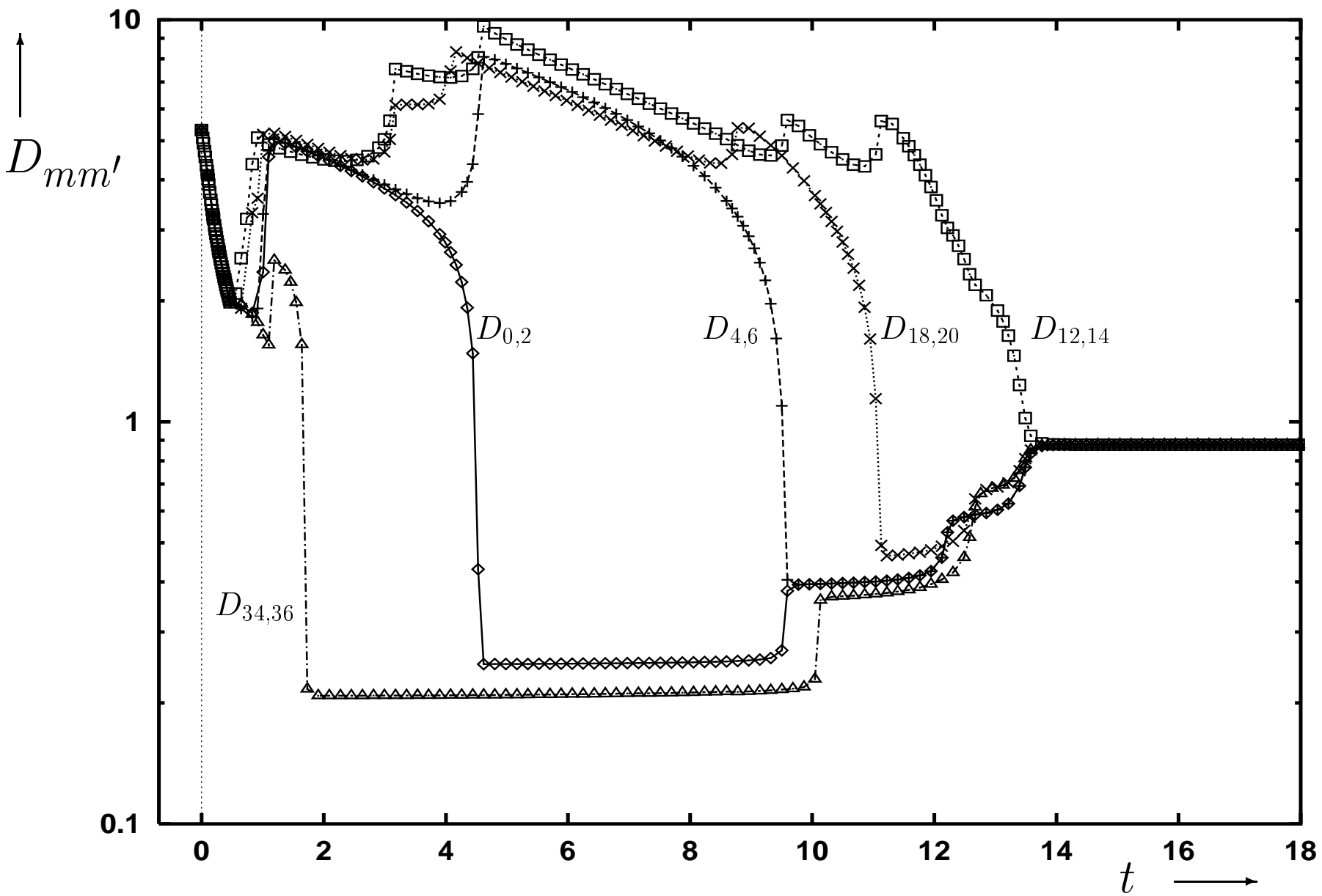


Fig. 14

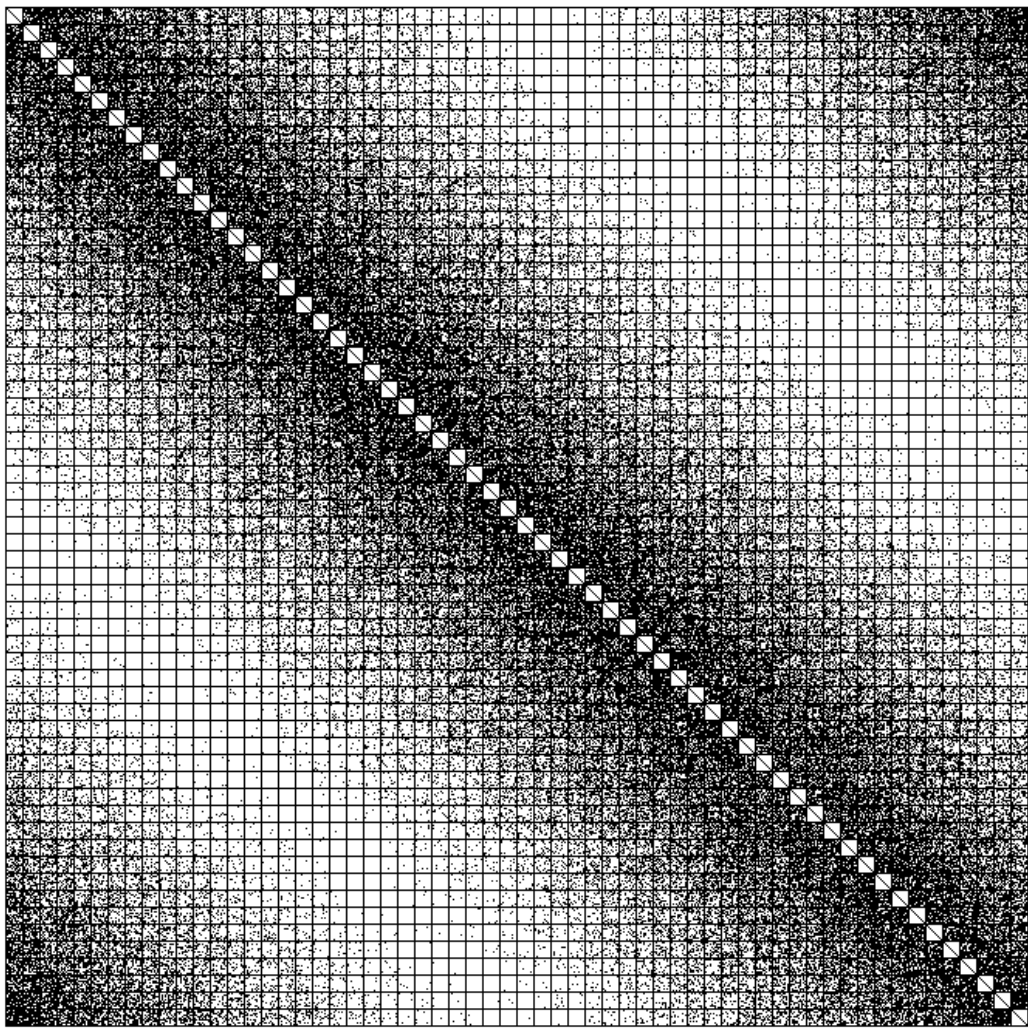


Fig. 4a

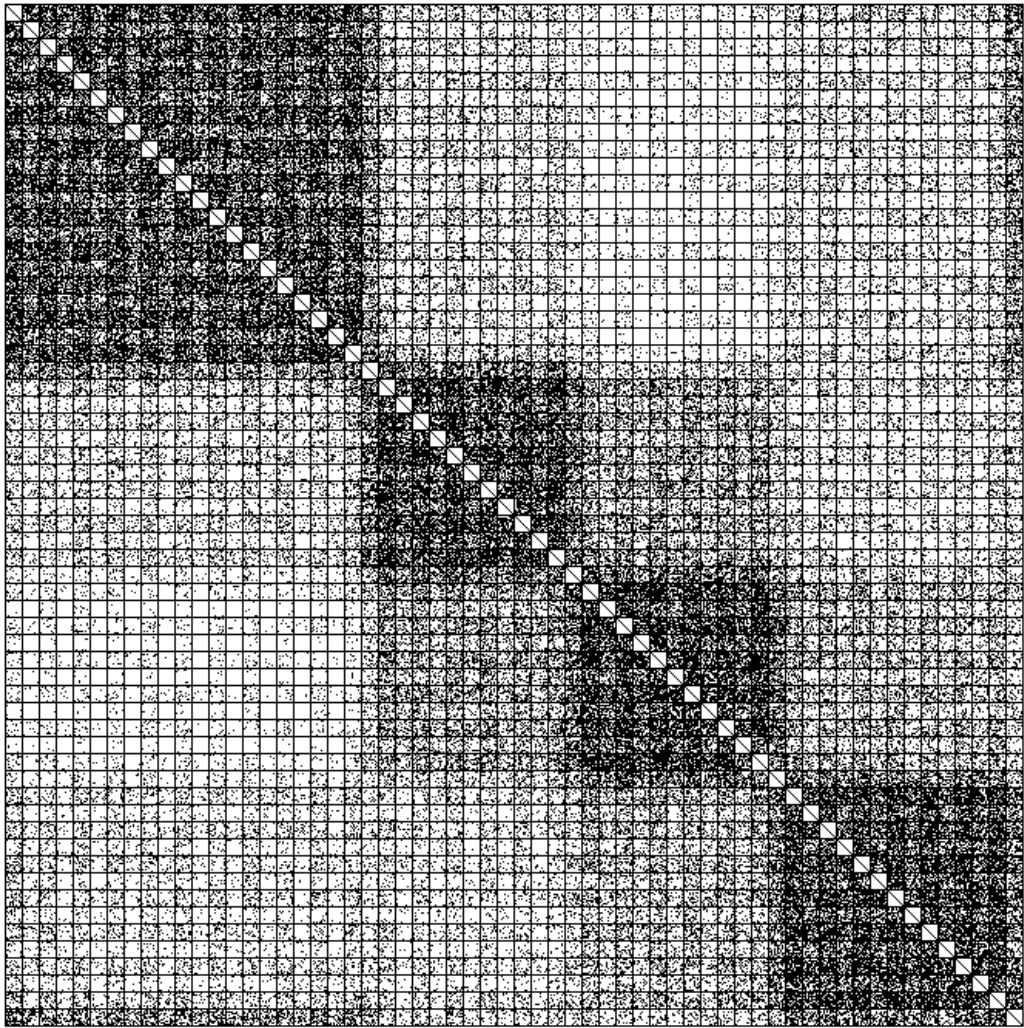


Fig. 4b

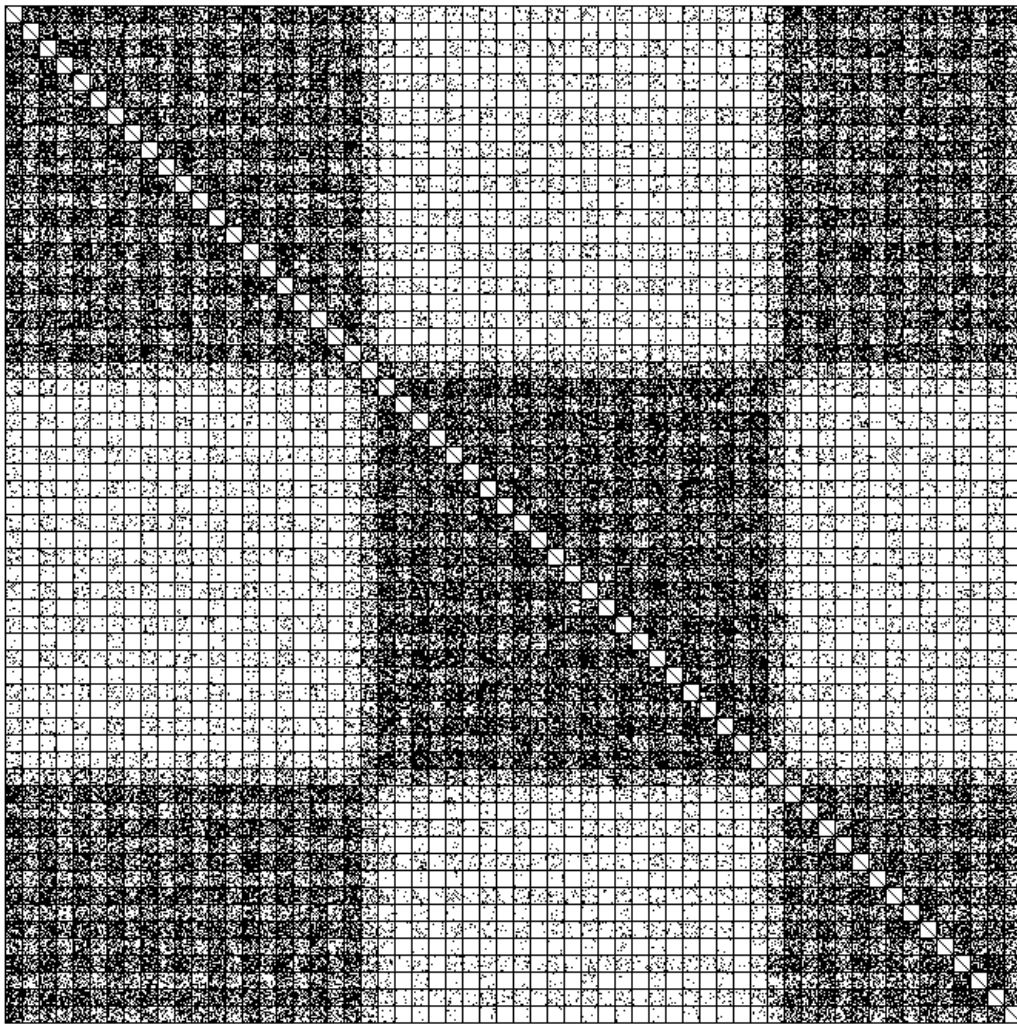


Fig. 4c

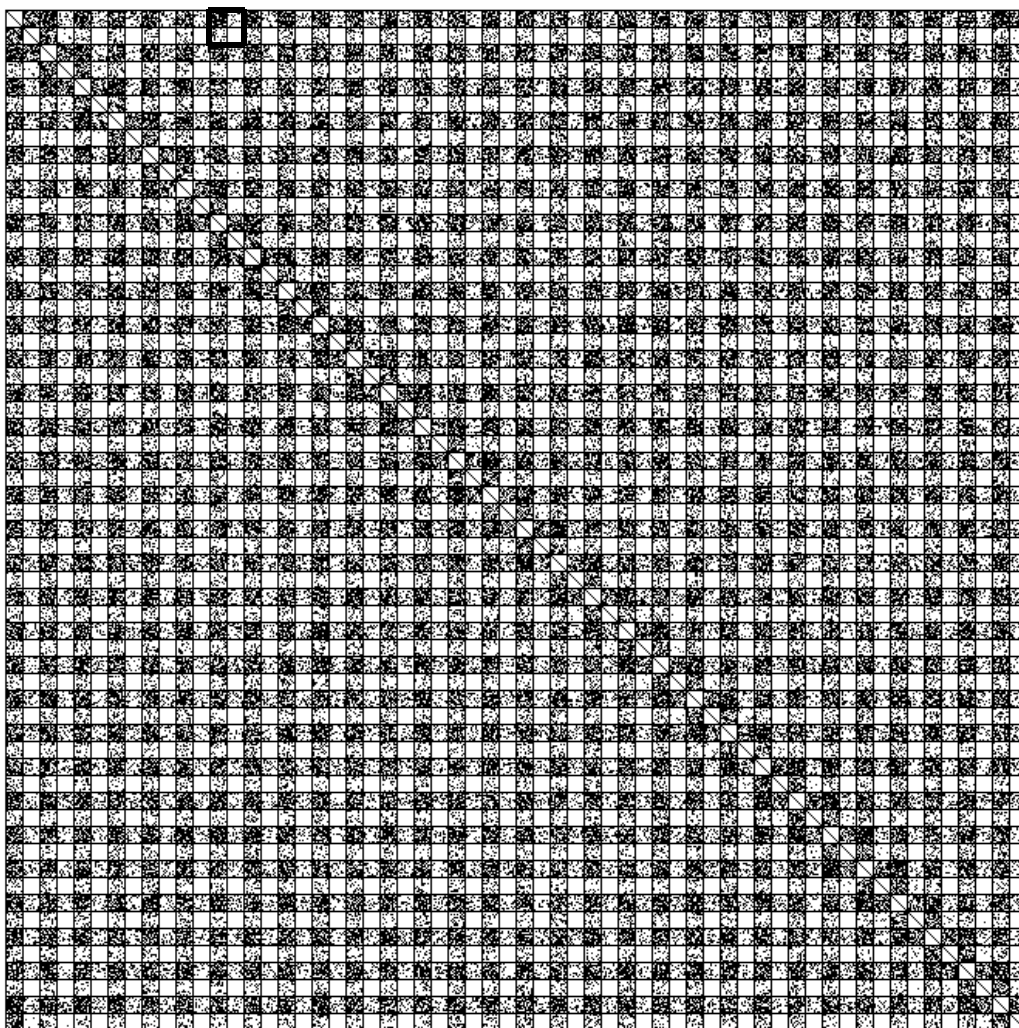


Fig. 4d

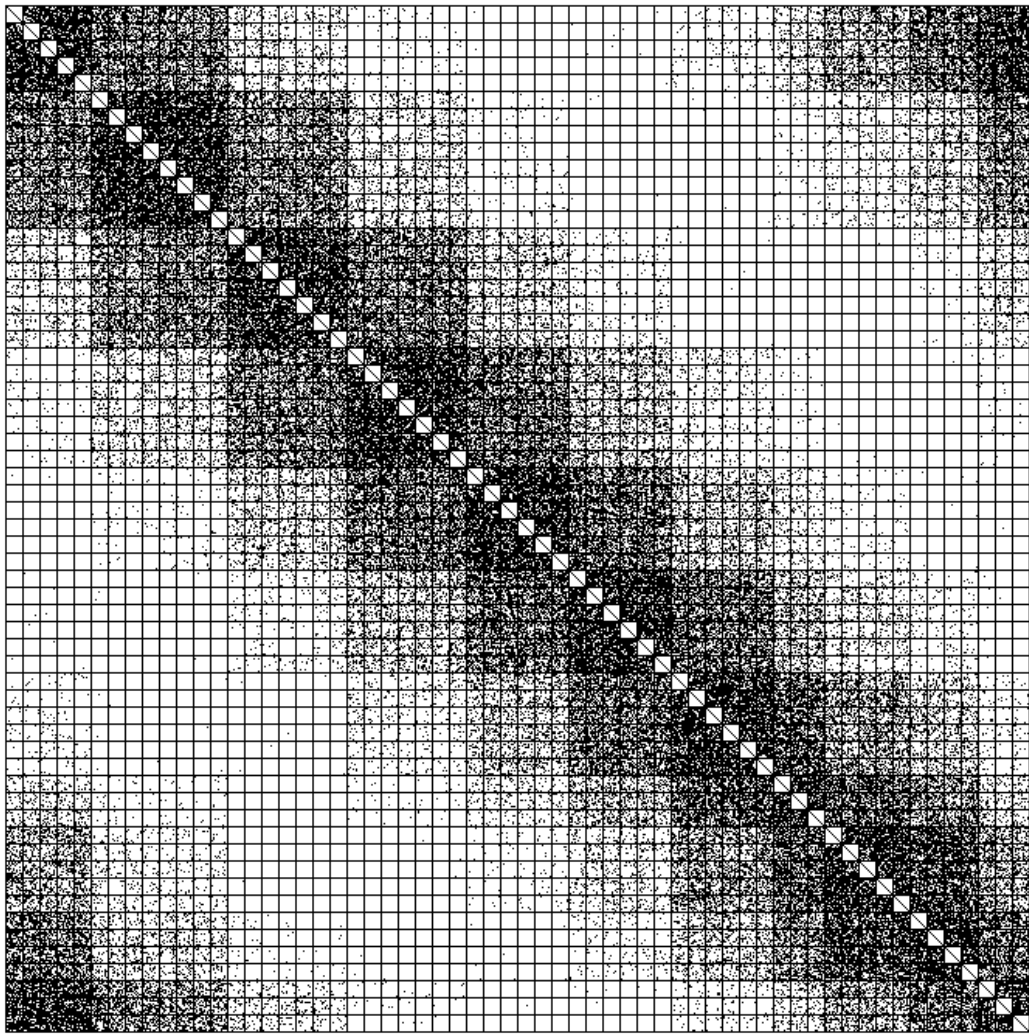


Fig. 15a

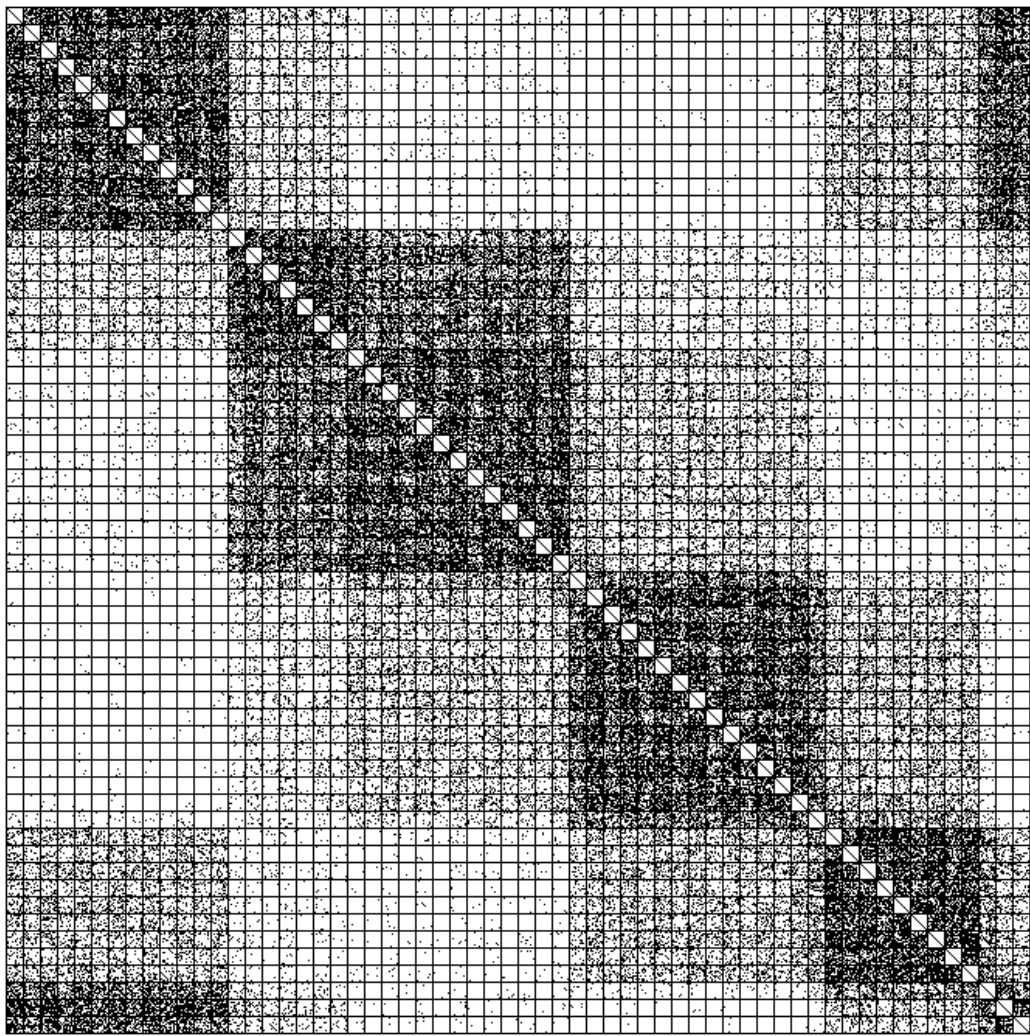


Fig. 15b

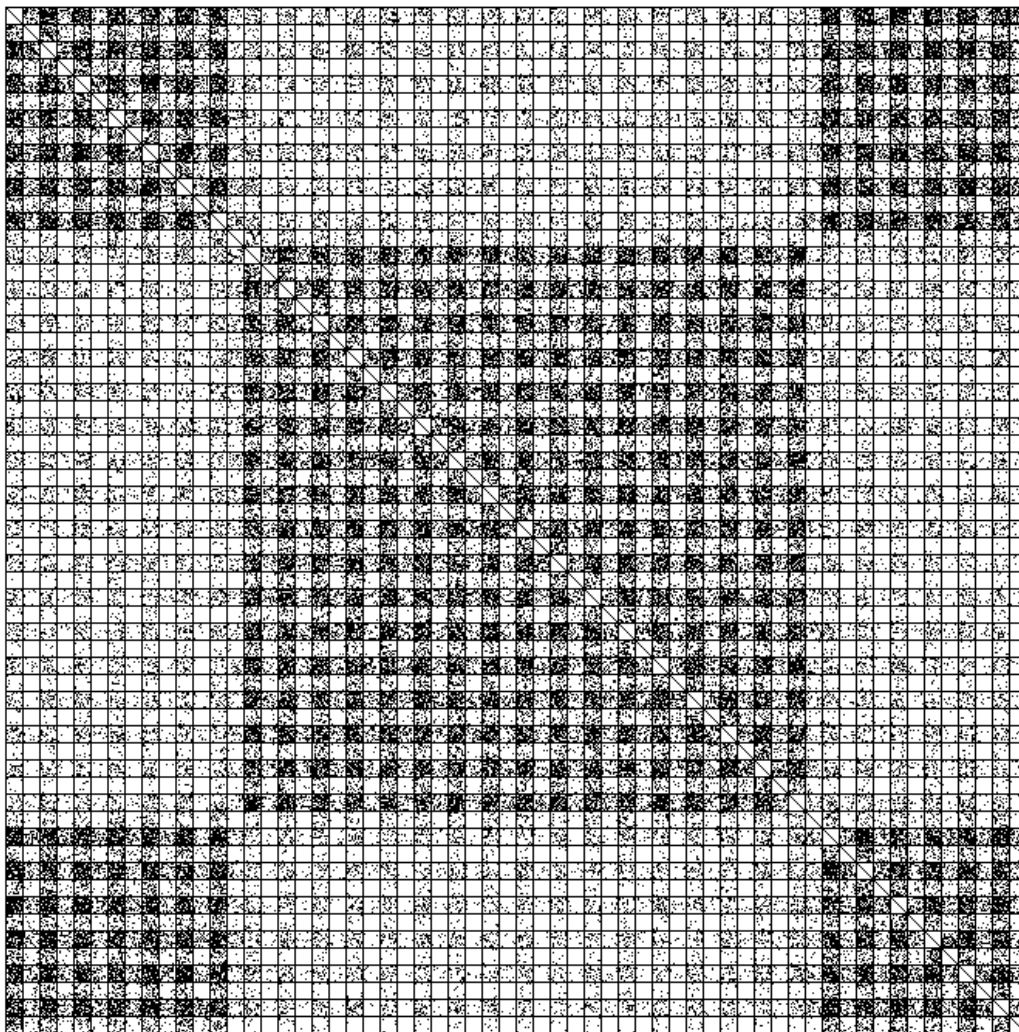


Fig. 15c